The Thesis Committee for Jordan Taylor Isbell
Certifies that this is the approved version of the following thesis:

Using Huff n' Puff with a Recycled Hydrocarbon Gas as a Means for Enhancing Oil Recovery in a Liquid-Rich Shale Reservoir

APPROVED BY
SUPERVISING COMMITTEE:

Supervisor:

Kishore K. Mohanty

Ryosuke Okuno

Using Huff n' puff with a Recycled Hydrocarbon Gas as a Means for Enhancing Oil Recovery in A Liquid-Rich Shale Reservoir

by

Jordan Taylor Isbell, B.S.Ch.E.

Thesis

Presented to the Faculty of the Graduate School of

The University of Texas at Austin

in Partial Fulfillment

of the Requirements

for the Degree of

Master of Science in Engineering

The University of Texas at Austin

August 2016

Dedication

This thesis is dedicated to my parents, sister, and grandparents. You all made me the man that I am today, and for that I am eternally grateful.

Acknowledgements

First and foremost, I would like to thank Dr. Kishore Mohanty for his guidance throughout my two years here at The University of Texas. Working for someone who is not only a world-class researcher, but also a world-class teacher was by far the most important part of my experience here. I also want to thank Dr. Ryosuke Okuno for his contributions to my research and expertise of the subject matter herein. Thanks as well to Dr. Matt Honarpour, Dr. Ed Turek, and the rest of the group at BHP Billiton for funding this project and also advising me throughout its entirety. Without you all, this work would not have been possible.

I would also like to extend a special thank you to two of Dr. Mohanty's research staff members: Dr. Eric Dao and Dr. Chammi Miller. Chammi was always there for me when it came to understanding the analytical techniques involved in my experimental work, and Eric was always there for me when it came to fixing the many leaks I had throughout my experiments. Thanks as well to Dr. Peixi Zhu, who helped me immensely in improving my understanding of reservoir simulation. I also owe a special thanks to Daryl Nygaard down in the machine shop for always being there to tweak and customize the many parts in my experimental setup.

Thank you as well to all of the members of Dr. Mohanty's research group. From lunches at Kinsolving with Pinaki and Himanshu to our weekly research meetings, you all were essential to my success and keeping me motivated throughout my time here. A special thanks also goes out to Barb Messmore for always getting on me when I forgot to send in my research updates.

Lastly and most importantly, I want to think all my friends in Austin, especially my roommates, Colin Schroeder and Matthew Ramos. You all helped me enjoy graduate school to its fullest and truly made it an experience that I will never forget.

Abstract

Using Huff n' puff with a Recycled Hydrocarbon Gas as a Means for Enhancing Oil Recovery in A Liquid-Rich Shale Reservoir

Jordan Taylor Isbell, M.S.E.

The University of Texas at Austin, 2016

Supervisor: Kishore K. Mohanty

In recent years, production in unconventional reservoirs has increased exponentially due to technological breakthroughs in horizontal well completions. However, even with new technology, ultimate recovery after primary production in these reservoirs is extremely low (5-10% of original oil in place). The huff n' puff process is considered to be a strong candidate for enhancing these notoriously-low recovery factors in unconventional reservoirs, especially those that are liquid-rich, in a cost-effective manner. Huff n' puff is an enhanced oil recovery method in which one well alternates between injection, soaking, and production. Gas injection is often used in this scenario because of its high injectivity compared to water and its ability to develop miscibility with the reservoir oil. In this work, a recycled hydrocarbon gas was used due to its ease of accessibility within the target reservoir.

In this work, the application of huff n' puff to a liquid-rich shale reservoir with nanodarcy-range permeability was investigated both experimentally and numerically. A completely unique experimental setup was fabricated in order to execute oil recovery

experiments on preserved core plugs taken from the target reservoir. In these experiments, it was shown that significant amounts of oil could be recovered after two huff n' puff cycles lasting approximately one day each. Using propane as the injection gas resulted in higher recoveries when compared to the recycled gas due to enhanced miscibility with the oil. It was also shown that the ratio between soaking pressure and production pressure is a significant factor in recovering oil via huff n' puff. An additional cycle was run with a longer soaking time, but no additional oil was recovered.

A set of numerical reservoir models was also created to further investigate the recovery mechanisms in the huff n' puff process. Lab-scale models were created in an attempt to replicate the experimental findings. The results showed that the recoveries seen in the experiments and simulations were very similar. Also, as long as injection took place above MMP, it was shown that the gas and oil mixed similarly in all cases regardless of pressure. Furthermore, lower production pressures allowed for more gas expansion and therefore better recovery, proving that production pressure alone may be an important parameter rather than the ratio between production and injection pressures. Field-scale models were also created. These models also showed that gas expansion plays a significant role in recovering oil. However, there were several key differences associated with sweep efficiency and the use of live oil versus dead oil.

Table of Contents

List of Tables

List of Figures

CHAPTER 1: INTRODUCTION

Unlike conventional reservoirs, shale reservoirs are ultra-low permeability formations that do not readily allow fluid flow. In order to overcome this obstacle, wells are drilled horizontally and then stimulated by multiple hydraulic fractures. Due to this new method of drilling, hydrocarbon production in unconventional reservoirs has increased exponentially over the past 8 years. The Eagle Ford shale in southeastern Texas, for example, went from a cumulative production rate of 352 bbl/day in 2008 to 838,293 bbl/day in early 2014 (Railroad Commission of Texas, 2013). However, due to the ultra-low permeability, production rates of most horizontal shale wells decline sharply after a short period of time – sometimes by as much as 70% in the first year alone (Hoffman, 2012). Furthermore, the ultimate primary recovery factor for shale wells is on the order of 5-10% OOIP (Hoffman, 2012). There has been a great deal of work done recently to attempt to improve recovery. Conventional waterflooding techniques cannot be applied due to the low injectivity of water, but gas injection may be a viable alternative because of its low viscosity. Gas injection, such as CO_2, has shown success for years in conventional reservoirs; as of 2010, the US was producing around 300,000 bbl/day from gas injection, and that number is likely higher now (Hoffman, 2012).

Gas injection offers several advantages that may prove to be beneficial in unconventional reservoirs. As mentioned previously, the viscosity of gas is much lower than that of water, making it easier to inject and use as a displacement fluid. In addition to this, gas can also be injected as a supercritical fluid if the pressure and temperature of the reservoir is suitable. For example, CO_2 is in the supercritical phase at pressures above 1,070 psi and temperatures above 88^o F. The density of supercritical CO_2 is approximately 70% that of water, and the kinematic viscosity is approximately 10-25% that of water (Chen and

Zhang, 2010). When injected as a supercritical fluid at high enough pressures, miscibility between oil and gas can also be achieved, therefore forming a single phase. In this situation, the oil can be transported with the supercritical gas and therefore achieve higher recovery, much like the mechanism behind surfactant chemical enhanced oil recovery (Chen et al, 2014). This mechanism is especially interesting in terms of potential use for unconventional enhanced oil recovery because the pressures and temperatures typically found in these reservoirs may be conducive to achieve miscibility.

Conventional injector-producer schemes may not be feasible in unconventional reservoirs. Even with close well-spacing, the ultra-low permeability of the shale matrix could cause the pressure propagation to take a considerably long amount of time. Therefore, it might be advantageous to adopt a single-well injection-production scheme known as "huff 'n' puff." In this approach, gas is pumped into the fractured horizontal well and then shut-in, allowing the gas time to migrate into the matrix and mix with the oil. After this shut-in period, the well is then reopened to produce at a lower pressure, which causes the single-phase gas/oil mixture to expand and flow out. This process can then be repeated in a cyclic manner to further increase recovery.

In today's low-price environment, it is of the utmost importance to maximize efficiency during oil production. As production quickly declines in a shale oil well, drilling new horizontal wells with an estimated cost of 8 to 16 million USD per well (Jacobs, 2015) was once a viable option to generate more cash flow. This option is not profitable in the current situation, though. As a result, many companies will look to refracture existing wells. However, at an estimated cost of 1 to 3 million USD per refracturing job (Jacobs, 2015); this option appears too risky for many companies considering the inconsistent field results and lack of expertise on the subject. Gas injection, therefore, is a strong candidate for enhancing oil recovery in existing shale oil wells. The following body of work will

investigate, both experimentally and numerically, the viability of using a recycled hydrocarbon gas in a liquid-rich shale (LRS) reservoir as a means of enhancing oil recovery.

CHAPTER 2: LITERATURE REVIEW

This chapter serves as an overview of other works that have been done in the area of miscible gas flooding. Section 2.1 describes the underlying fundamentals like phase behavior, ternary diagrams, and the determination of minimum miscibility pressure. Much of this section is derived from *Fundamentals of Enhanced Oil Recovery* by Larry W. Lake, Russell T. Johns, William R. Rossen, and Gary A. Pope (Lake et al, 2014). Section 2.2 then goes on to examine various works that have studied the use of miscible gas injection in unconventional reservoirs.

2.1 Miscible Gas Injection

Miscible gas flooding, or in a broader sense, solvent flooding is one of the oldest and most widely used methods of enhancing oil recovery; since 2002, it has produced more barrels of oil in the US than all other EOR methods combined (Lake et al, 2014). Miscible gas flooding is a recovery technique that relies on the mass transfer that occurs when miscibility develops between the gas and reservoir oil (Lake et al, 2014). Miscibility is defined as the physical condition in which two fluids are able to mix in all proportions without the formation of an interface (Clark et al, 1958). Miscibility can either be experienced at first contact (first-contact miscibility) or developed as the crude continuously mixes with the injection gas (multiple-contact miscibility). Besides pressure, miscibility is determined by intermediate hydrocarbon content of the reservoir oil and temperature. The gases used in the field vary widely based on accessibility and economic conditions. In general, CO2 and various hydrocarbon gases are cheap, easily accessible, and are therefore the most popular gases being used currently in the US (Dao et al, 2005).

The properties of the injection gas are of the utmost importance when it comes to the performance of the gas flood. Due to the large mobility ratio, there will always be substantial sweep efficiency issues. Therefore, an injection gas with a viscosity and density as close to that of the reservoir oil as possible will yield the best results. Moreover, light oils are most suitable for gas injection processes. Aside from rheology, another important property of the injection gas is how it mixes with the reservoir oil. In order to classify this property, ternary diagrams are used. Gardner et al. (1981) goes into detail about how these diagrams are used to describe the mixing of different crude oils with CO_2. Figure 2.1 shows an example of a CO_2-crude oil ternary diagram. Because crude oil often contains many components, it is common practice to split the system into light, intermediate, heavy *pseudocomponents*. Water is often ignored in solvent flooding, acting as an inert component with respect to phase behavior. As shown in Figure 2.1, there is 2-phase region that exists where the composition of the mixture contains low levels of the intermediate pseudocomponent. Therefore, as stated earlier, the composition of the crude is very important to obtaining miscibility. In Figure 2.1, the crude contains mostly heavy components, so the dilution line must cross through the 2-phase region. This is an example of developed miscibility because the CO_2 and crude must mix and re-equilibrate several times before the single-phase region can be reached. The assumption that the system mixes in a series of well-mixed cells is indeed an oversimplification of the complex mixing process that occurs within the reservoir, but is adequate for understanding the fundamentals of miscibility attainment.

It is important to note that ternary diagrams contain information only for constant pressure and temperature. In reservoir-scale gas injection processes, though, the pressure is constantly changing as production or injection ensues. Therefore, it is important to determine the minimum pressure at which miscibility occurs, or MMP. MMP is the most

frequently reported characteristic of gas flooding phase behavior, and is quantified through various methods like slim tube experiments, mixing-cell methods, the method of characteristics, and various other experimental processes. Slim tube experimentation is the most widely-used direct measurement method, but can be very time consuming. Mixing-cell methods and the method of characteristics are numerical methods so they can be completed quickly, but are dependent on the accuracy of the EOS being used.

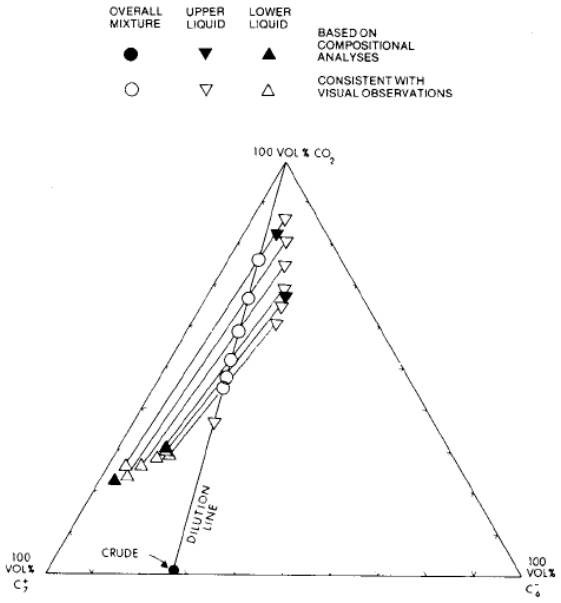

Figure 2.1: Ternary equilibria for CO_2-recombined Wasson crude at 2000 psi and 105°F (Gardner et al, 1981).

In most instances, reservoir conditions do not allow for the attainment of miscibility, and even when it is attained, it is usually only a short distance from the injector. Therefore, immiscible displacement mechanisms have merit when considering gas injection processes. These processes include limited vaporization and extraction, oil viscosity reduction, oil swelling, solution gas drive, and interfacial tension lowering. It is important to emphasize that these mechanisms are not entirely immiscible because some mass transfer takes place between phases. Oil recovery is therefore quite complex in gas

injection processes as pressure approaches MMP because miscible displacement happens concurrently with the immiscible displacement mechanisms described above. The primary goal of this work is to investigate how these mechanisms occur within liquid-rich shale reservoirs. For more information, one can refer to Chapter 7 of *Fundamentals of Enhanced Oil Recovery* (Lake et al, 2014) and *Theory of Gas Injection Processes* by Franklin M. Orr, Jr. (Orr, Jr., 2007).

2.2 Miscible Gas Injection in Liquid-Rich Shale Reservoirs

Although recovery through miscible gas injection is a relatively well-understood process in conventional reservoirs, there is still a lot of discovery to be done when applying it to LRS reservoirs. For example, if permeability is too low then pressure drops in the near-wellbore region might be too high to achieve miscibility. Furthermore, small pore sizes have been shown to affect phase behavior and MMP significantly (Teklu et al, 2014).

Fragoso et al. (2015) studied the use of recycled gas and dry gas injection in shales through numerical simulation. This work used compositional single porosity, dual porosity, and dual permeability simulations to study the possibility of injecting gas into an oil-containing shale formation. Relative permeability curves for the matrix system were adopted from Honarpour et al. (2012) and straight line relative permeability curves were used for the fracture system. Diffusion was also taken into account in these simulations through the use of Sigmund correlations for gas and oil diffusion coefficients. Along with the three different models, each model was run with two different injection techniques: continuous gas injection and huff 'n' puff gas injection. For the huff 'n' puff injection technique, each cycle consisted of 100 days of injection followed by 100 days of production.

The single porosity model served as the baseline model where only shale matrix is present around the hydraulic fractures. In this model, the permeability was varied from the starting permeability of 250 nd, all the way up to 0.01 md in order to study the effect that it has on gas injectivity. Two different gas compositions were also used: one with only methane, and another with 70% C_1, 20% C_3, and 10% C_6. Injection of these gases was started after 5 years of primary production, which was shown to be the optimal starting time. The results for the single porosity model are summarized in Table 2.1. As shown, for a permeability of 250 nd, no additional oil is recovered with gas injection. The results are very similar for a permeability of 0.001 md, but when the permeability is increased to 0.005 md, significantly more oil is recovered. These results indicate that there is likely a permeability threshold that must be determined for gas injection into shale matrices. Furthermore, in the higher permeability cases, significantly more oil was recovered through the injection of the hydrocarbon gas mixture compared to 100% methane, which is likely caused by the hydrocarbon gas mixture being more miscible with the oil and having a lower saturation pressure.

Table 2.1: Single porosity simulation results. Continuous gas injection was started 5 years after primary production (Fragoso et al, 2015).

Matrix Permeability	Primary Recovery (%)	Recovery by CH4 injection (%)	Recovery by (70% C1 + 20%C3+ 10%C6) injection (%)
250 nd	5.25	5.25	5.25
0.001 md	7.04	7.28	7.72
0.005 md	8.94	10.72	13.55
0.01 md	9.39	13.21	16.80

Shale formations are often naturally fractured, making the dual porosity and dual permeability models the most suitable for modeling flow in a matrix/fracture system. The permeability and porosity values were kept constant at the values described previously, and as in the single porosity model, different compositions of gas were tested. Different starting

times for gas injection were also evaluated. The results of the dual porosity and dual permeability models, along with the 0.01 md single porosity model, are summarized in Table 2.2. In the dual porosity and permeability cases, the natural fracture permeability was 0.04 md. Table 2.2 shows that, on average, huff 'n' puff outperformed continuous injection in the dual porosity and dual permeability models. Whereas in the single porosity model, continuous injection performed slightly better. Additionally, it can be concluded that injection fluid composition does not have significant effects on performance until C6 is added. In all models, a significant jump in recovery was shown in the cases where C6 was used in the injection gas. This alludes to the fact that these cases might be achieving some degree of miscibility, whereas the other cases are not.

Table 2.2: Simulation results for the 0.01 md single porosity model and dual porosity and permeability models (Fragoso et al, 2015).

		Gas Injection		
Model	**Primary Recovery**	**Injected Fluid**	**Continuous Gas Injection**	**Huff and Puff**
Single Porosity	9.39	Methane	13.21	12.82
		95% C1 + 5% C2	13.43	12.76
		80% C1 + 20% C2	14.26	12.79
		70 % C1 + 20 % C3 + 10% C6	16.80	15.42
Dual Porosity	10.62	Methane	15.83	26.29
		95% C1 + 5% C2	16.08	26.47
		80% C1 + 20% C2	17.26	27.08
		70 % C1 + 20 % C3 + 10% C6	40.63	32.55
Dual Permeability	10.03	Methane	18.22	19.66
		95% C1 + 5% C2	18.85	19.88
		80% C1 + 20% C2	20.52	20.54
		70 % C1 + 20 % C3 + 10% C6	32.83	20.96

Fragoso et al. (2015) concludes that dual permeability models are necessary to accurately reflect performance of gas injection processes in naturally fractured shales, and that the presence of natural fractures greatly enhances recovery. In shales without natural fractures (single porosity), there is a minimum permeability that must be carefully quantified before choosing to implement gas injection. Injected fluids that can achieve

miscibility with the reservoir oil produce much better results than lean gas, but availability and economics may be limiting factors in the use of these fluids. Finally, it was concluded that huff 'n' puff outperformed continuous injection in terms of oil recoveries, and is much more economically feasible since only one well is needed for injection and production.

It is traditionally thought that unlike conventional reservoirs where convection is the dominating mass transfer mechanism, diffusion may be a significant driving force in miscible gas injection in fractured LRS reservoirs. The diffusion process is described by Fick's Law,

$$N_i = -D_i \nabla c_i \qquad \text{(Eq. 2.1)}$$

which states that the molar flux of component *i* is proportional to the concentration gradient of component *i.* The diffusion coefficient, D_i, is a proportionality constant and varies by temperature and pressure. In the case of gas flooding in shales, the concentration gradient of oil is created through miscibility. When the gas penetrates the shale matrix above MMP, it mixes with the oil in a single phase. After this mixing occurs, an oil concentration gradient is formed between the gas in the shale matrix containing solubilized oil, and bulk gas in the fracture that does not contain oil. This then drives the oil out of the matrix and into the fracture, where it can then be recovered (Hawthorne et al, 2013). Along with this mechanism, there are also several others at play that may contribute to enhanced recovery, such as pressure-driven advection, oil swelling, and oil viscosity reduction (Lake et al, 2014). The aim of this section is to review the numerical and experimental results of recent work done in this area in order to determine which mechanism(s) dominate.

Wan and Sheng (2015) developed a compositional model that coupled the diffusion equation into a dual-permeability. In this model, the species balance for Component *i* in an n_c-component system is given by Hoteit and Firoozabadi (2009) and Jamili (2010) in the following convection-diffusion equation:

$$\underbrace{\frac{\partial}{\partial t}\left(\sum_j \phi\rho_j S_j \omega_{ij}\right)}_{\text{accumulation}} + \nabla\cdot\left(\underbrace{\sum_j \rho_j \omega_{ij}\vec{u}_j}_{\text{convective flux}} + \underbrace{\sum_j J_{i,j}}_{\text{diffusion flux}}\right) = 0,$$
$$i = 1, \ldots, nc \quad j = o,\ g \tag{Eq. 2.2}$$

The velocity for each phase is described by Darcy's law, and the diffusion follows Fick's law. Therefore, the governing matrix- and fracture-flow equations of the diffusion model are given as

$$\left[\frac{\partial}{\partial t}\left(\sum_j \phi\rho_j S_j \omega_{ij}\right)\right]_m + \nabla\cdot\left[\sum_j (\rho_j \omega_{ij}\vec{u}_j + J_{i,j})\right]_m + \sum_j \tau_{mf,ij} = 0,\ \ i = 1, \ldots, nc\ \ j = o,\ g. \tag{Eq. 2.3}$$

$$\left[\frac{\partial}{\partial t}\left(\sum_j \phi\rho_j S_j \omega_{ij}\right)\right]_f + \nabla\cdot\left[\sum_j (\rho_j \omega_{ij}\vec{u}_j + J_{i,j})\right]_f - \sum_j \tau_{mf,ij} = 0,\ \ i = 1, \ldots, nc\ \ j = o,\ g. \tag{Eq. 2.4}$$

There are $2\times(2n_c+4)$ equations in this dual-permeability model: $2n_c$ come from Equations 2.3 and 2.4 and $2n_c$ can be derived from the thermodynamic equilibrium equations. The rest come from the mass-fraction-conservation equation, capillary pressure equation, and saturation equation in the matrix and fracture. This model is therefore inherently different from previous model because it includes the matrix-fracture mass transfer due to diffusive flux for both oil and gas. To validate the model, Wan and Sheng (2015) compared the numerical simulation results with experimental data and published numerical simulation results.

In this work, as with Fragoso et al. (2015), recycled natural gas is used as the injection gas. The composition is 70% C1, 20% C3, and 10% C6. Also, a continuous gas

injection scheme was used by modeling two hydraulically-zipper-fractured horizontal wells. Table 2.3 summarizes the reservoir properties for the model input. The bottom-hole pressure of the producing well was set to a minimum value of 2000 psi, which is close to the MMP. Figure 2.2 compares the results of the simulations with Coats (1989), which used identical inputs, but only accounted for gas diffusion between fracture and matrix. In Figure 2.2a, the two results closely resemble one another because of the high permeability (1 md), but in Figure 2.2b, the results differ significantly. This confirms that matrix/fracture diffusion in the oil phase is significant in ultra-low permeability reservoirs where convection is greatly hindered, which is why the Coats model vastly underestimates recovery in the 0.0001-md case.

Gas injection rate was also studied in this work. Figure 2.3 shows oil recovery vs. pore volumes of gas injected (PVI). It is shown in this plot that a slower injection rate results in higher recovery after 1 PVI. This can again be explained by diffusion: if the injected gas flows at a high interstitial velocity, then there is less residence time for oil in the high concentration side to diffuse to the low-concentration side. However, Figure 2.4 shows that oil recovery will be higher with respect to time when the injection rate is higher, resulting in a trade-off that would need to be evaluated from an economic standpoint.

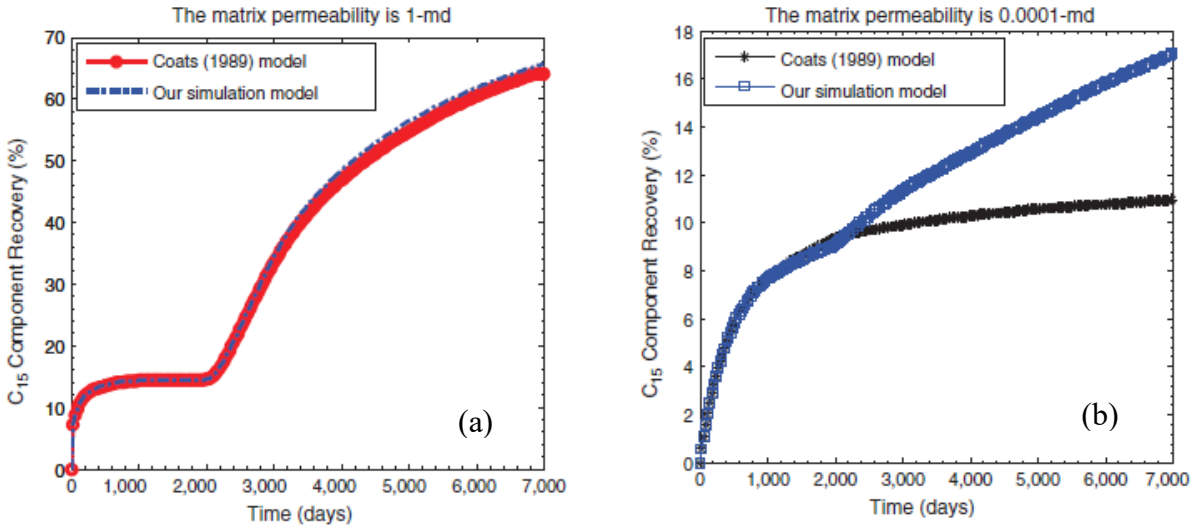

Figure 2.2: Comparison of Wan and Sheng (2015) to Coats (1989) in (a) 1 md reservoir, and (b) 0.0001 md reservoir (Wan and Sheng, 2015).

Table 2.3: Reservoir properties for the model input (Wan and Sheng, 2015)

Initial Reservoir Pressure	6,425 psi
Reservoir Temperature	160°F
Saturation Pressure	2,302 psi
Rock Compressibility	5.0×10^{-6} psi^{-1}
Porosity	6%
Permeability of shale matrix	100 nd

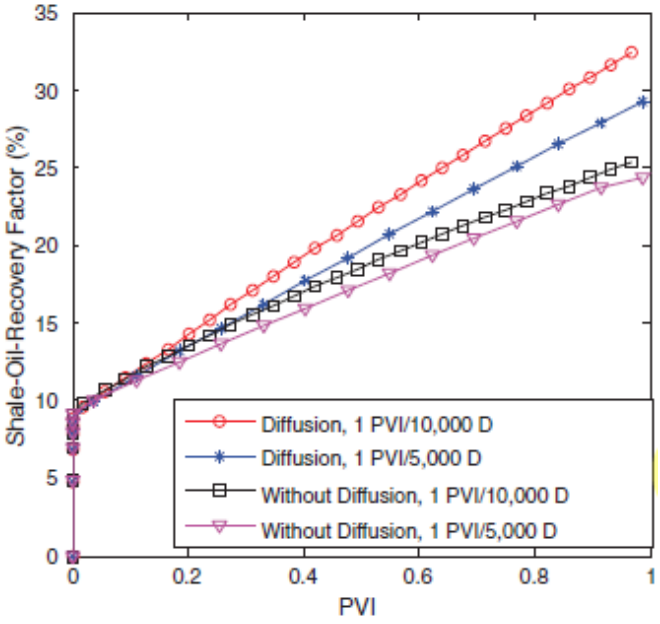

Figure 2.3: Oil recovery vs. PVI (Wan and Sheng, 2015).

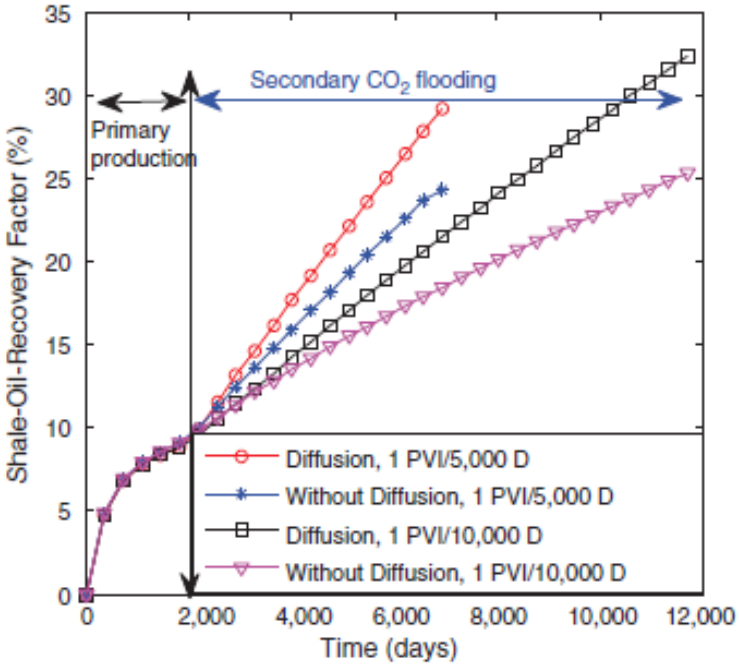

Figure 2.4: Oil recovery vs. time (Wan and Sheng, 2015).

In recent years, there has been a significant increase in the amount of numerical work on gas huff 'n' puff processes in unconventional reservoirs. However, there is still a need to develop effective methods for experimental work in order to validate these models. Kovscek et al. (2008) and Vega et al. (2010) tested the performance of CO_2 injection in a fractured siliceous shale core with a permeability of 0.02-1.3 mD. However, there have been very few tests done on un-fractured and ultra-low permeability shale samples.

Hawthorne et al. (2013) did some experimental work to study oil recovery mechanisms shale reservoir core plugs treated with CO_2. The Middle Bakken samples used in this study had porosities ranging from 4.5% to 8.1% and permeabilities from 0.002 to 0.04 md. The Upper and Lower Bakken samples used did not have data available, but it was thought that permeabilites were orders of magnitude lower compared to the Middle Bakken samples. All CO_2 injections were performed at reservoir conditions of 5000 psi and 230^o F. The rock samples were placed into the 10-mL extraction cell, but were not sealed to the cell wall in any way, which is unlike conventional coreflooding procedures. This allows the CO_2 to flow free around the sample rather than be forced through it in order to mimic the tendency for CO_2 to flow through fractures rather than the shale matrix. The high-pressure CO_2 was pumped into the top of the cell, and exited through the bottom to a heated flow restrictor at a rate of 1.5 mL/min. The effluent of the flow restrictor was then collected in order to measure hydrocarbon recovery. In this study, the outlet was left open to run continuously for some tests, therefore mimicking continuous injection of CO_2, and for other tests it was opened and closed cylically in order to mimic the huff 'n' puff process. The results of these tests were then compared to one another.

Figure 2.5 shows the results for huff 'n' puff tests in which the CO_2 was left static in the cell except for 10-minute "production periods," where the cell was allowed to flow (while maintaining temperature and pressure) in order to collect extracted hydrocarbons.

The Lower Bakken tests recovered significantly less oil than the other tests, which is due to the fact that these samples had much lower permeability values than the other samples. Another interesting result in this work was the preference of lower molecular weight hydrocarbons to be extracted over higher molecular weight hydrocarbons. This is likely due to the fact that lower molecular weight hydrocarbons are more miscible with the oil, so when the single oil/gas phase is formed, there will tend to be a disproportionate amount of lighter hydrocarbons in this phase.

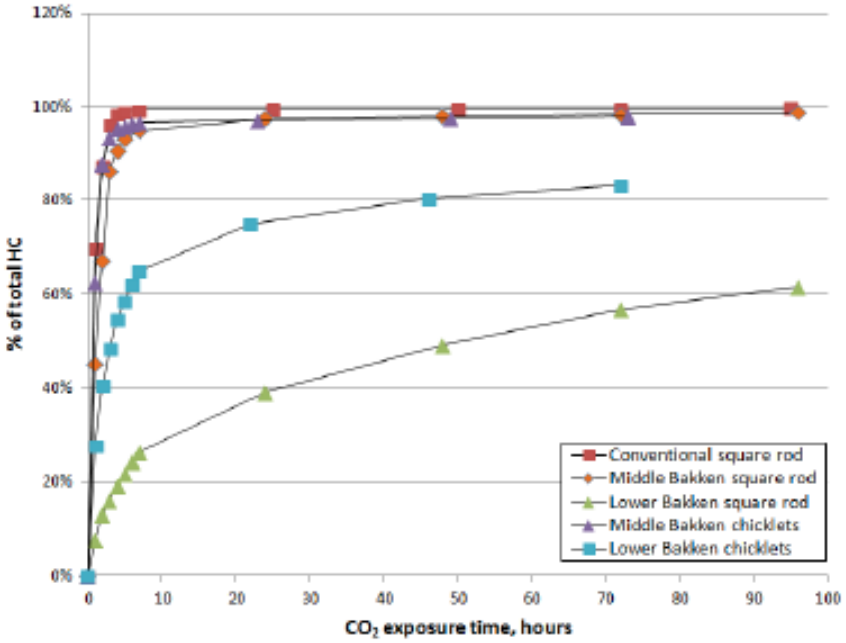

Figure 2.5: Oil recovery vs. time for CO2 huff ‘n’ puff tests done on Middle and Lower Bakken and conventional reservoir rock samples with 96 hours of exposure time (Hawthorne et al, 2013).

Yu and Sheng (2016) conducted similar experiments with Eagle Ford core samples using nitrogen as the injection gas. In this work, the core samples were saturated with dead oil and tests were ran to investigate the effects of flooding time and injection pressure on recovery. Unlike Hawthorne et al. (2013), the samples in this work were confined in a

coreholder and the nitrogen was forced through the sample like a conventional coreflood. Flooding time ranged from 1 day to 5 days in increments of 1 day, and injection pressure ranged from 1,000 psi to 5,000 psi in 1,000 psi increments. X-ray CT was also used to visualize phase flow and estimate the recovery efficiency during the tests.

The results from Yu and Sheng (2016) show recovery factors ranging from 10% to 35%. The samples in this work had porosities around 5% and permeabilities around 70 nD, which was measured using a complex transient measurement system. In the injection time investigation, it was found that approximately 50% of total production occurred within the first day of injection. The gas broke through after 8 hours of flooding and the outlet flow rate became stabilized in one day, both of which are earlier than expected. This points to possible channeling occurring in the core plug and explains the poor performance after the first day. In the injection pressure investigation, the results showed higher recovery factors at high injection pressures. This is based on the fact that increased pressure creates extended flow channels and improves conductivity. However, applying high pressure in the field is not recommended as it would increase costs and make oil production less economical.

Sun et al. (2016) did both experimental and numerical work on CO_2 injection in liquid-rich shale (LRS) reservoirs with complex fracture networks. The experimental work was described in the work by Tovar et al. (2014). Two sets of experiments were performed using preserved core samples: one at 3000 psi (above MMP) and 150°F and the other at 1600 psi (below MMP) and 150°F. The core samples, which were approximately 2.5 cm in diameter and 3.5 cm in length, were placed in a core holder with glass beads surrounding the sample. The purpose of these glass beads was to imitate the presence of a highly permeable fracture around the sample. A Computed Tomography (CT) scanner was used to monitor the saturation variations within the cores during the experiments. The results

indicated that CO_2 constantly penetrated into the cores throughout the entirety of the experiments, which lasted two to three days on average. Based on the estimated OOIP, the experiments yielded high oil recovery.

The main focus of Sun et al. (2016) was to numerically model the core-scale laboratory experiments described above. A dead oil fluid model was used with a 3D Cartesian grid, which contained a matrix portion surrounded by a highly permeable fracture portion. Both sets of experiments were modeled (3000 psi and 1600 psi), plus an extra case was modeled at 1800 psi, which is considered "near miscible" conditions. The results shown in this work state that diffusion plays a significant role in core-scale simulations. The recovery factor is sensitive to matrix and fracture porosity, saturation, and diffusion coefficient, while matrix permeability, fracture permeability, relative permeability, and capillary pressure do not significantly affect it. This differs from field-scale simulations where porosity, permeability, time of first injection, cycling length, injection rate, injection pressure, and number of cycles all play a significant role in producing incremental oil. Capillary pressure, length of soaking time, and diffusion coefficient were not significant in the field-scale simulations. It is finally concluded that lab-scale simulations are highly dependent on diffusion, whereas field-scale simulations rely on gas expansion more heavily than diffusion. Because of this, field-scale huff n' puff is most effective below the bubble-point pressure, which is also hypothesized by Sanchez-Rivera (2014).

2.3 Concluding Remarks

Miscible gas injection is the most complex of solvent flooding techniques used to enhance oil recovery. This is due to the many different recovery mechanisms at play, each of which may vary in significance on a case-by-case basis. The process of miscible gas

injection recovers oil through the mixing of the injection gas with the crude oil, which causes several advantageous phenomena such as the reduction of oil viscosity, oil swelling, interfacial tension lowering, and even the formation of an entirely miscible phase. As shown in Section 2.1, the rheology of the gas as well as the phase behavior of the gas-crude oil system need to be fine-tuned in order to develop an effective miscible gas flood. The measurement of minimum miscibility pressure (MMP) is a key parameter for miscible gas flooding because it gives a minimum pressure needed to develop a significant amount of miscibility between the two fluids.

There has been a fair amount of studies done recently that explore the use of miscible gas injection in liquid-rich shale (LRS) reservoirs. As stated in Chapter 1, the ultimate recovery in these reservoirs is typically very low due to permeabilities often in the nanodarcy range. Gas injection is therefore a viable solution in these reservoirs because of its high injectivity, especially the huff n' puff scheme. Huff n' puff uses a single horizontal well to inject the gas, let it mix with the oil, and then produce back. Applying miscible gas injection to LRS reservoirs differs from conventional applications in several ways. Teklu et al. (2014) states that small pore sizes significantly affect phase behavior and MMP. Fragoso et al. (2015), Wan and Sheng (2015), and several others (Zhu et al, 2015; Sanchez-Rivera et al, 2015; Sanchez-Rivera, 2014; Hoteit, 2011) have numerically modeled gas injection processes in shale reservoirs. In these studies, several key parameters were investigated to better understand how the recovery mechanisms in LRS reservoirs differ from conventional reservoirs. It is shown that diffusion may play a significant role in the mixing of the oil and injection gas because convection cannot occur in ultra-tight matrices. This could be possible on the microscopic scale, but in the field scale it is likely that convection (through hydraulic and natural fractures) still dominates the mixing process.

Injection schemes (huff n' puff vs. fracture-to-fracture), production and injection pressures, and injection fluids were also investigated.

Far less experimental work has been done in this field (Hawthorne et al, 2013; Yu and Sheng, 2016; Sun et al, 2016) because of the difficulties associated with shale experimentation. These studies showed that quantifying the recovery of oil in lab-scale gas injection experiments could be done several different ways, such as mass measurements, CT number, and GC analysis. Hawthorne et al. (2013) and Sun et al. (2016) studied huff n' puff experiments while Yu and Sheng (2016) studied conventional flooding experiments. All results showed that injection above MMP yielded significantly better recoveries than below. However, there were few significant conclusions made about how injection pressure, production pressure, or any other parameters effect experimental performance. Experimental results are necessary to learn more about applying this process to LRS reservoirs because the numerical models involve many limitations that likely lead to unrealistic results. The primary goal of this work, therefore, is to build on the limited experimental work being done in the field of miscible gas injection in shales.

CHAPTER 3: FIELD BACKGROUND, MATERIALS, METHODOLOGY, AND DATA ANALYSIS

The following chapter serves as a premise for the results given in Chapter 4. In this chapter, all pertinent information regarding the target reservoir will be given along with a description of the fluids and core samples used. Following this section, a description of all equipment used in the experimentation and analysis phases of this study will be given. Finally, the methodology behind each experiment and analytical process will be described.

3.1 Field Background

The target reservoir in this study is a liquid-rich shale (LRS). Liquid-rich shales are both the source and the reservoir for the hydrocarbon liquids, with the source represented as organic-rich matter that is finely interbedded with the calcite or quartz clay-rich grains. The fluid storage is mainly within the organic-rich material while the inorganic matrix and natural fracture network provide the conduit for flow. LRS reservoirs are typically heterogeneous and anisotropic, and also vary from strongly oil-wet to mixed-wet. TOC can vary between 1% and 15% with different levels of maturity, which results in oil API gravities ranging from 30 to 55 degrees and GORs ranging from 300 to 10,000 scf/stb. Like any other type of shale reservoir, matrix permeabilities can often be in the nanodarcy range with pore sizes usually less than 20 nm, which is near the molecular size of the large liquid components. Because of this, unconventional fluid flow behavior is often observed, with a preference for the lighter components to flow compared to the heavier ones (Clarkson et al, 2011).

The reservoir temperature and pressure, combined with the composition of the crude, are such that miscibility between crude and injection gas is thought to be attainable.

Moreover, convenient supply of light hydrocarbon gases makes this reservoir an ideal candidate for gas injection as a means of enhancing oil recovery. Table 3.1 shows a complete summary of all pertinent reservoir information, which was obtained both independently and from Gong et al. (2013). The target reservoir is thought to be very heterogeneous, containing extensive natural fracture systems in the most productive zones. So, it is important to note that the pressure, porosity, and permeability values listed are all average values, and can vary greatly within the reservoir.

Table 3.1: Summary of all pertinent reservoir information (Gong et al, 2013).

Formation Type	Shale	
Average Depth	11,000	feet
Temperature	257	°F
Pressure (average)	7,200	psi
Porosity (average)	7%	
Permeability (average)	500	nD

3.1.1 RESERVOIR FLUIDS

The reservoir fluids include the reservoir oil and injection gas. The reservoir oil used was a dead oil with an API gravity of ~40° API. At ambient conditions, the viscosity and density of the oil are ~1.8 cP and ~0.82 g/cm^3 (~51 lb$_f$/ft^3), as shown in Figures 3.1 and 3.2. The P-T diagram for this laboratory oil is shown in Figure 3.3. The proposed injection fluid is a recycled gas produced from a gas zone within the same reservoir, and is approximately 62 mol% C_1, 18 mol% C_2, 10 mol% C_3, and 10 mol% C_4. It has a critical temperature and pressure of 67°F and 1500 psi, respectively, which allows for supercritical behavior in all experiments. Figure 3.4 shows the viscosity of this gas as a function of pressure at various temperatures, which was modeled via the Peng-Robinson equation of state using the QNSS/Newton 2-phase flash calculation method. For comparison's sake, Figure 3.5 shows a plot from Goodrich (1980) of CO_2 viscosity. At an injection pressure

of 4000 psi and at reservoir temperature, the recycled gas has a viscosity roughly 4% of that of the lab oil, while CO_2 has a viscosity roughly 6% of that of the lab oil.

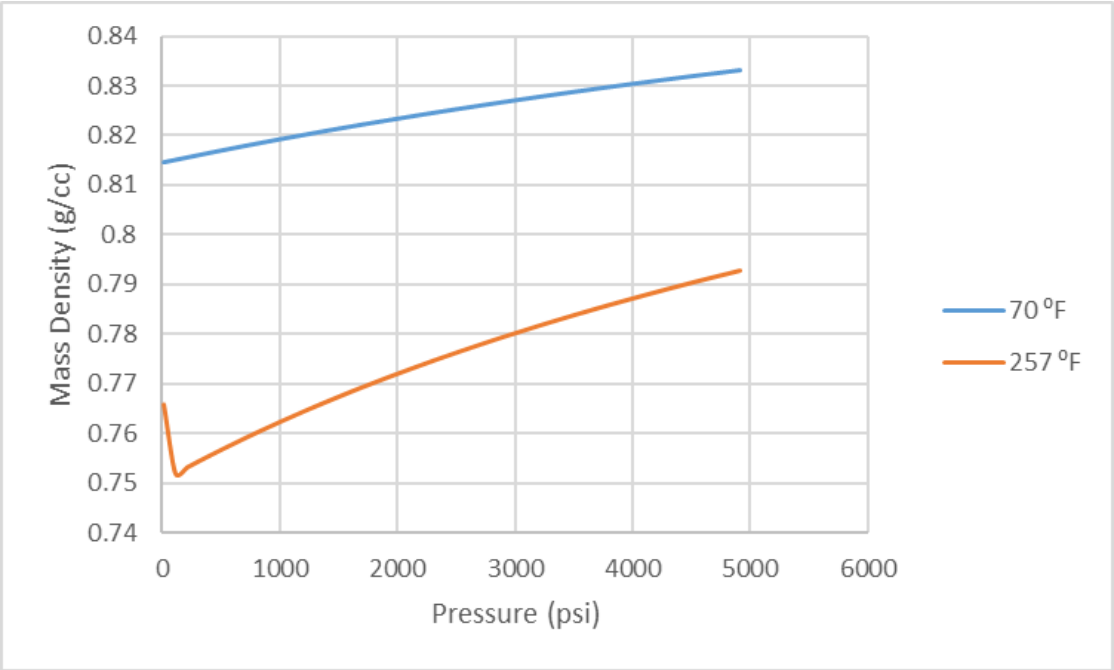

Figure 3.1: Mass density of the laboratory oil used in all experiments at room and reservoir temperatures.

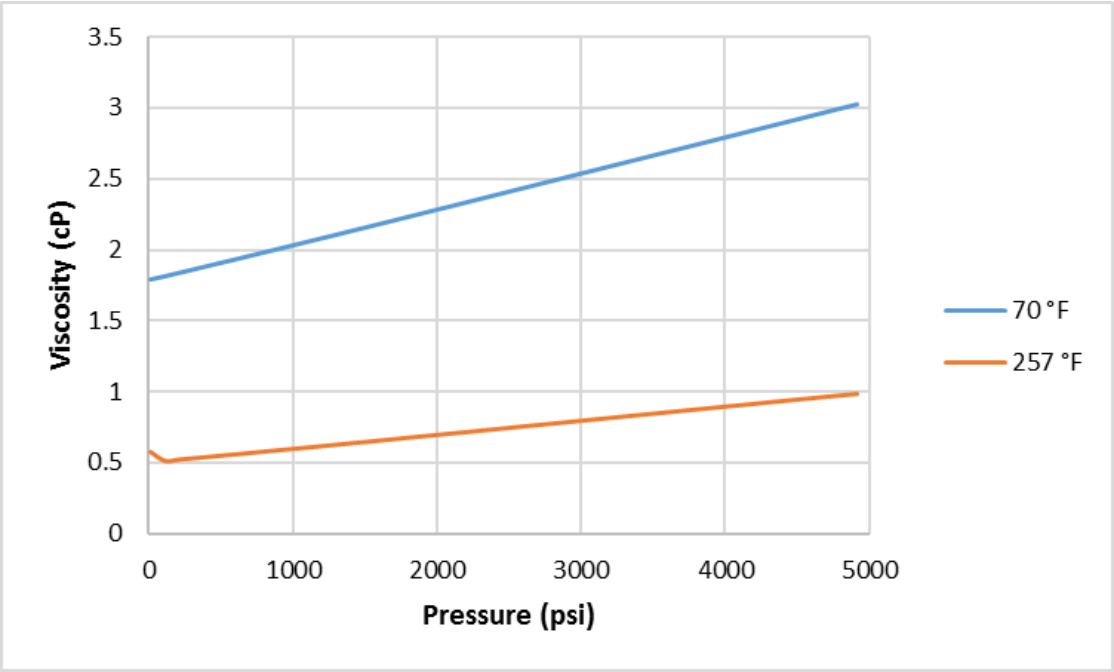

Figure 3.2: Viscosity of the reservoir oil used in all experiments at room and reservoir temperatures.

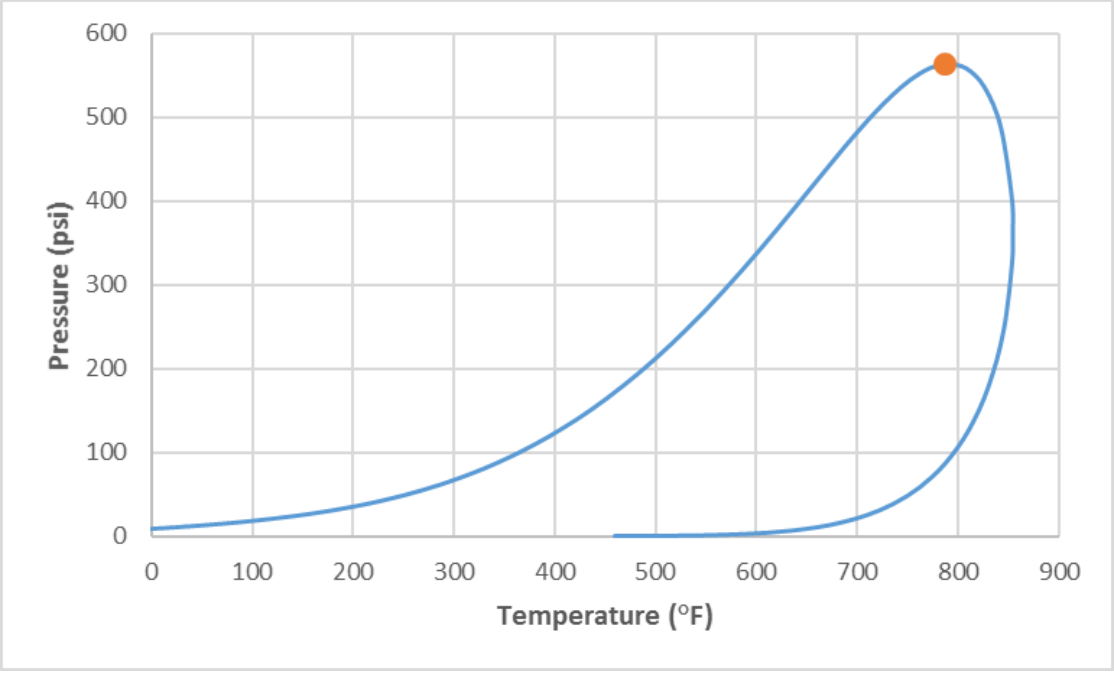

Figure 3.3: P-T diagram for the laboratory oil.

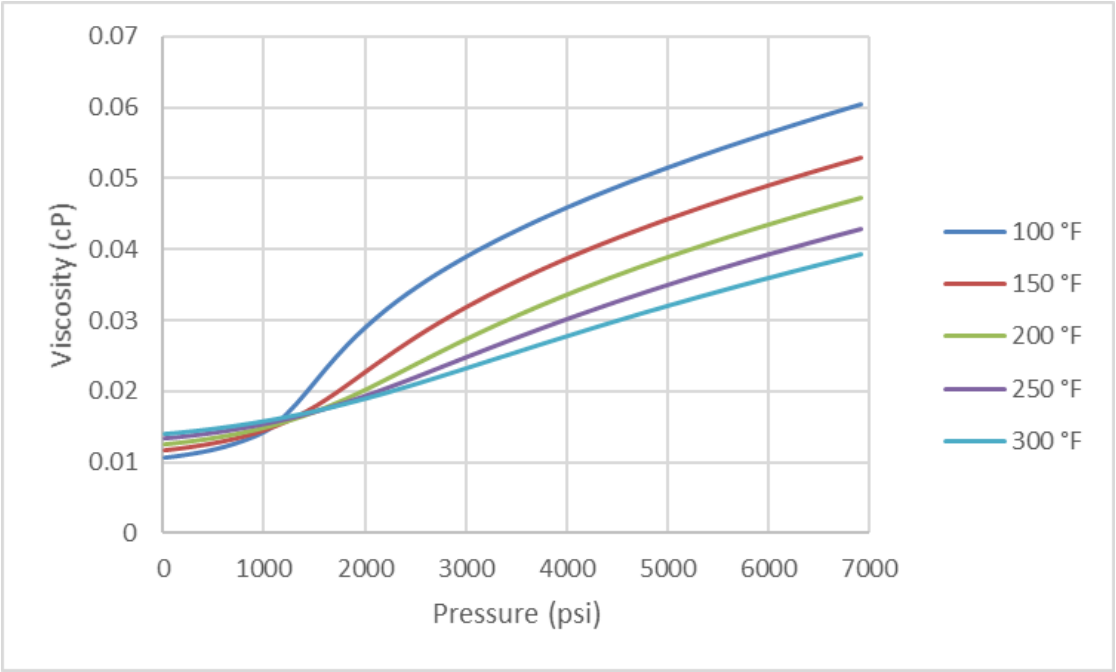

Figure 3.4: Viscosity of the recycled gas as a function of pressure at various temperatures.

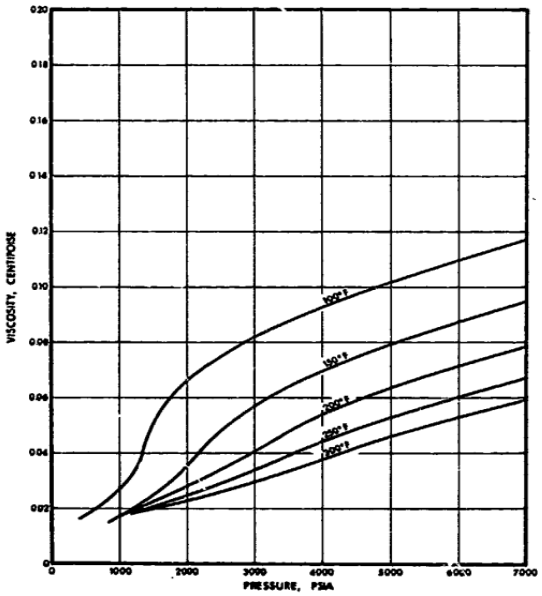

Figure 3.5: Viscosity of CO2 as a function of pressure at various temperatures (Goodrich, 1980).

3.1.2 CORE SAMPLE ANALYSIS

The core samples used in this work were preserved reservoir samples, meaning that once the cores were brought to surface they were immediately vacuum sealed and coated with a heavy wax layer to preserve most of the in-situ reservoir fluids. The methods used to analyze these samples included x-ray diffraction (XRD), scanning electron microscopy (SEM), nuclear magnetic resonance (NMR), and solvent extraction. These methods provided crucial qualitative and quantitative data describing mineralogy, porosity, pore-size distribution, matrix and fracture structures, and fluid saturations.

XRD Analysis

X-ray diffraction (XRD) was used to analyze the mineralogy of the core samples in this study. The shale reservoir of interest in this work consists mostly of calcite, but also has a significant clay composition. Additional tests were also conducted to determine the total organic content (TOC) of the samples, which came out to be about 5.5 wt% on average. Table 3.2 shows the results of the XRD analysis.

Table 3.2: XRD analysis for the shale samples.

Mineral	Wt%
Calcite – $CaCO_3$	55.89
Dolomite – $CaMg(CO_3)_2$	0.78
Siderite – $FeCO_3$	0.09
Anhydrite – $CaSO_4$	0.68
Fluorapatite – $Ca_5(PO_4)_3F$	0.07
Quartz – SiO_2	17.47
Albite – $NaAlSiO_8$	7.29
Pyrite – FeS_2	2.57
Marcasite – FeS_2 (White)	0.06
Illite - $(K,H_3O)(Al,Mg,Fe)_2(Si,Al)_4O_{10}[(OH)_2,(H_2O)]$	7.66
Kaolinite - $Al_2Si_2O_5(OH)_4$	1.74
Chlorite - $(Mg,Fe)_3(Si,Al)_4O_{10}(OH)_2\cdot(Mg,Fe)_3(OH)_6$	1.98
Montmorillonite - $(Na,Ca)_{0.33}(Al,Mg)_2(Si_4O_{10})(OH)_2\cdot nH_2O$	3.71
Total Clay	15.1

SEM Analysis

The core samples were analyzed using an Environmental Scanning Electron Microscope in order to qualitatively identify the structure of the samples at a microscopic level. Figures 3.6 through 3.9 show the results of this analysis. These images show significant presence of calcite, clay, and pyrite minerals.

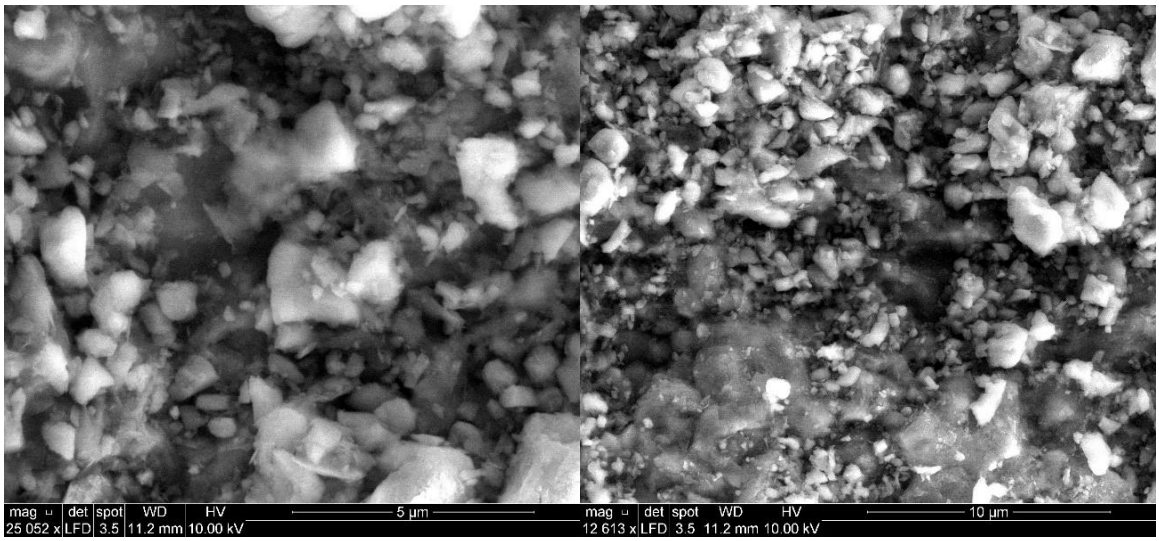

Figure 3.6: ESEM images of a shale sample, 5-µm scale (left) and 10-µm scale (right).

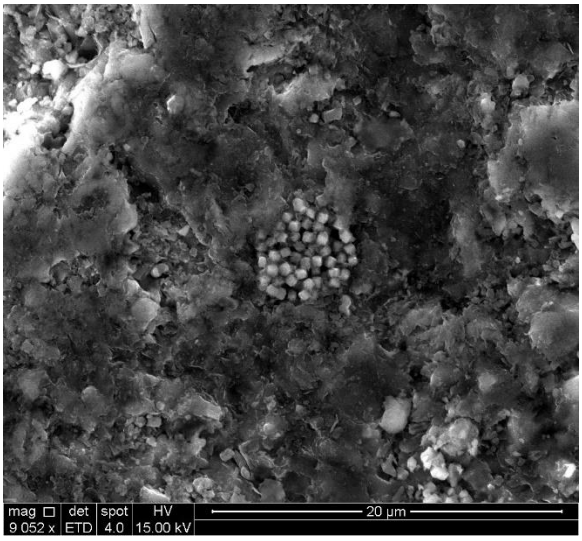

Figure 3.7: 20-µm ESEM image showing a pyrite crystal (middle).

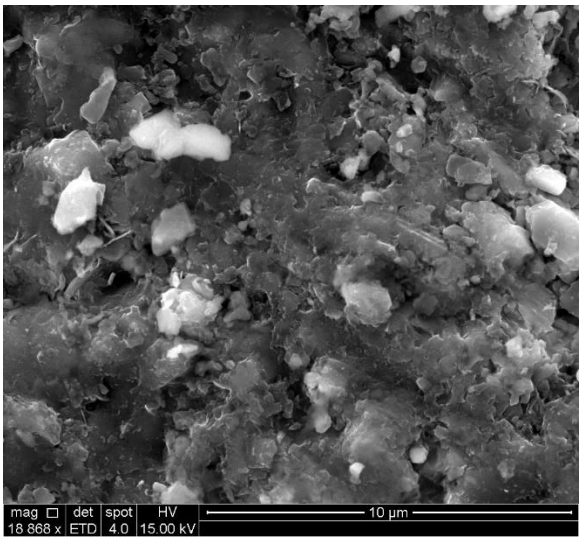

Figure 3.8: 10-µm ESEM image showing an abundance of calcite crystals (shown as the white particles).

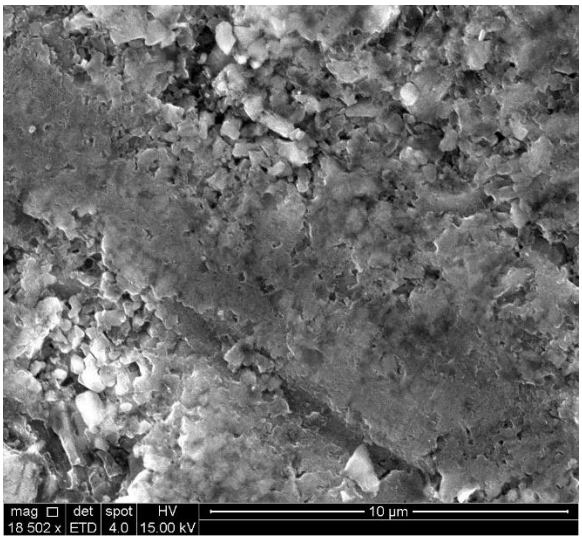

Figure 3.9: 10-µm ESEM image showing clay minerals (middle) with some calcite crystals (white particles).

NMR Analysis

The goal of the NMR analysis was to quantify porosity, pore-size distribution, and fluid saturations of the core samples. NMR analysis uses magnetization to polarize the spins of hydrogen nuclei found in reservoir fluids. When exposed to a static magnetic field, B_0, hydrogen nuclei behave like microscopic bar magnets, aligning themselves in the direction of the magnetic field. However, when exposed to electromagnetic radio frequency pulses transverse to B_0, these hydrogen nuclei briefly tip away from the direction of B_0. The time that it takes the hydrogen nuclei to return to their aligned state is known as the relaxation time, T_2, and is a function of pore-size distribution, fluid properties, formation mineralogy, and molecular diffusion (Akhurt et al, 2009).

The major findings of this analysis can be seen in Table 3.3. It is assumed that when the cores were taken to the surface, a significant portion of the movable fluids escaped, leaving mostly bound fluids. Therefore, it was necessary to measure the NMR responses of the cores both "as-received" and re-saturated in order to accurately quantify the in-situ fluid saturations. The core plugs used in this study had a diameter of 1.5 in and length of 2 in. The T_2 distributions show that the samples had an average movable porosity of 4.2% with 2.9 PU being movable oil. When compared to actual reservoir data, which says that total average porosity is approximately 7%, it can be approximated that there is 2.8 PU of bound fluids (clay-bound water, adsorbed gas, adsorbed oil, etc.) in these samples.

Table 3.3: Summary of major findings in the NMR study.

Movable Oil (PU)	Movable Water (PU)	Total Movable Porosity (%)	Pore-Size Movable Oil (nm)
2.9	1.3	4.2	170

Solvent Extraction

Although NMR can accurately quantify porosity, the differentiation between fluid types can be difficult, especially in shales. Because of this, solvent extraction was used as a way of directly measuring "as-received" oil saturation. In this method, the shale samples were crushed and filtered to constant grain size using a 120-mesh sieve. After this, the samples were placed into glass vials containing toluene at an approximate ratio of 1:1 (mass of shale to mass of toluene) and then left in a 125°C oven for 5 days. This process allows any oil, movable or bound, to dissolve in the toluene, which can then be analyzed via gas chromatography (GC). Gas chromatography is used further in the experimental portion of this work, and will be explained in Section 3.3.2.

The crushed shale samples were treated with toluene in three separate vials. After treatment, the liquids from each vial were filtered and pipetted into 1-mL glass GC vials. Each GC run was repeated 5 times for consistency. The results of all the runs are shown in Figure 3.10. From these results, it can be approximated that the liquid extracts contained an average of 1.03 vol% oil. Using the recorded shale masses, solvent volumes, and assuming a porosity of 4%, the initial oil saturation could then be calculated. Final results of the solvent extraction analysis can be found in Table 3.4. The initial oil saturation of 0.45 differs slightly from the NMR results, which postulate that the saturation of bound fluids is approximately 0.40.

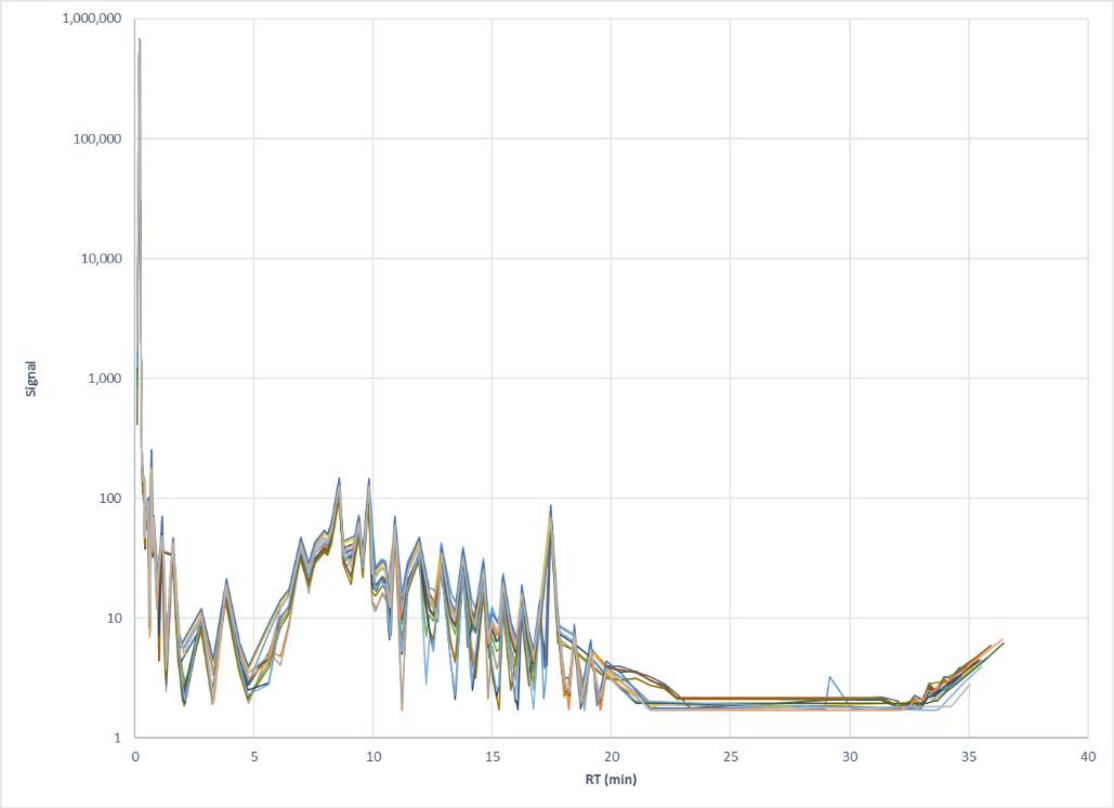

Figure 3.10: GC results for "as-received" crushed shale samples treated in toluene for five days.

Table 3.4: Averaged results of the solvent extraction analysis for "as-received" crushed shale samples.

Oil Extracted (mL)	0.06
Shale Mass (g)	9.80
Initial Oil Saturation, S_{oi}	0.45±0.07

3.2 Equipment

3.2.1 Experimental Equipment

The experiments in this study were all conducted using the setup shown in Figure 3.11, shown below.

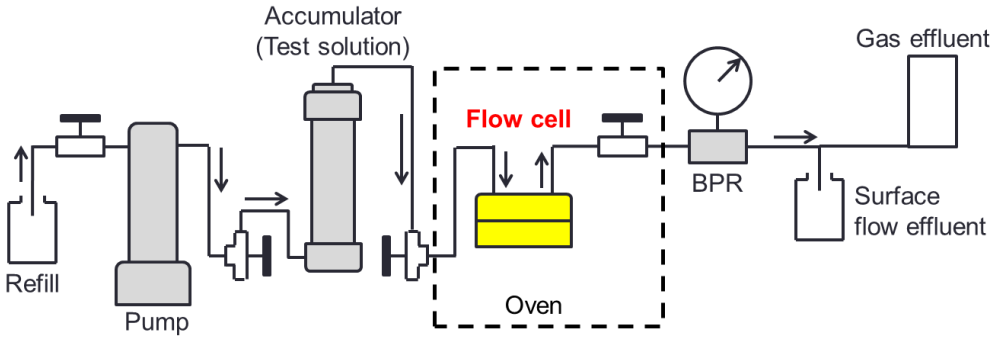

Figure 3.11: schematic diagram of the experimental setup.

Flow Cell

The flow cell was a custom-made, stainless steel pressure vessel capable of pressures exceeding 4500 psi and temperatures above 300 °F. It was the most important part of the experimental setup, as it was the vessel in which the shale sample is placed during experimentation. The shale sample was not confined by any overburden pressure like in conventional coreflooding techniques, but rather was open to let the gas flow freely around it. This is done intentionally to better mimic how the injection gas flows in the reservoir from the fracture into the matrix. The flow cell also had an inlet and outlet port equipped with high-pressure valves on the top that allowed for the gas to be injected into the vessel and "soaked" for a given amount of time, then flushed out during the production phase.

Oven

The oven used in these experiments was a Thermo Scientific Heratherm, which was capable of reaching 250°C.

Accumulator

The accumulator used in these experiments was a Hastelloy accumulator made by Vinci Technologies. It had a total volume of 1 L and was rated to 175°C and 700 bar (10,153 psi). The accumulator was used to deliver the injection gas to the flow cell.

Back-Pressure Regulator (BPR)

The BPR used in these experiments was made by Equilibar and was capable of maintaining 5000-psi pressure. It was used to maintain the soaking and production pressures within the flow cell.

Syringe Pumps

Two Teledyne Isco syringe pumps were used in these experiments (one for injection gas and one for BPR control/filling accumulator). These syringe pumps were capable of administering 7,500-psi pressure and had a total volume of 267 mL.

Custom Glass Vials

Glass vials capable of high temperatures and moderate pressures (50 psi) were custom-made for these experiments. These vials were used in effluent collection and treatment of the crushed shale samples. They were fitted with O-rings and polymer screw-caps so that no evaporation would occur during the treatment of the shale samples in toluene at 125°C.

3.2.2 Analytical Equipment

Gas Chromatograph

The gas chromatograph used in these experiments was an Agilent Technologies Model 7890A GC System. The column in this system was a DB-HT SimDis column with

dimensions of 5m length by 0.53 mm inner diameter. The stationary phase in the column was polysiloxane and the carrier gas was helium.

NMR

All NMR data was acquired on a GeoSpec2 rock core analyzer from Oxford Instruments at a resonance frequency of 2 MHz.

3.3 Setup and Procedure

Due to the lack of experimental research being done in the field of gas injection in shales, much of the setup and procedures in this work were fabricated solely by trial-and-error, and therefore changed significantly over the course of the study. For simplicity's sake, only the final iteration of setup and procedures will be discussed, in hope that they can be used and further revised in future work. The experimental portion of this work consisted of two phases: oil recovery experimentation, and post-experimental analysis of shale samples and effluent. The oil recovery experiments were all ran at constant pressure (and temperature) so that viscous displacement was absent.

3.3.1 Oil Recovery Experimentation

Mixing the Injection Gas

Mixing and loading the injection gas into the accumulator was a tedious process that involved a significant amount of time to complete. Before starting, it was necessary to calculate how much volume of each gas was necessary to achieve the desired composition. To do this, the molar volume of each gas was estimated at the desired conditions (ambient temperature, 4000 psi) using EOS simulation software. From here, a series of equations

derived from Equation 3.1, shown below, was solved to calculate the volumes of each pure component needed to make 1 L of injection gas.

$$z_i = \frac{V_i/v_i}{\sum_{i=1}^{4} V_i/v_i} \quad \text{(Eq. 3.1)}$$

In this equation, V_i is the desired volume of pure component i, v_i is the molar volume of component i at ambient temperature and 4000 psi, and z_i is the desired mole fraction of component i. Once the desired volumes of each component were calculated, the mixture process could then be started.

To mix the injection gas, two syringe pumps were needed: one filled with water and the other filled with the gas components. The process was started by vacuuming the side of the accumulator that the gas will go into, which should be on the bottom, while simultaneously filling the other side with water at the desired pressure of 4000 psi. After this, the gas-side valve was closed. The loading process was then started by filling the second syringe pump with C_4 and connecting it to the gas side of the accumulator. The pump could then be set to a constant flowrate and allow the desired amount of C_4 to be loaded into the accumulator at approximately 4000 psi. This process was then repeated for C_3, C_2, and C_1, making sure to periodically shake the accumulator in order to ensure good mixing. After completion of the loading process, the accumulator was then flipped over so that water could not leak into the gas chamber.

Re-saturating the Core Samples

In the first three experiments, the cores were re-saturated with the laboratory oil in order to better replicate in-situ fluid saturations. However, this process was exceedingly time consuming and was not continued in Experiments 4 and 5.

After mixing the injection gas and prepping the experimental equipment, the core sample was weighed, measured, and placed in the flow cell. After that, a second

accumulator was filled with the laboratory oil and connected to a secondary Isco pump. Re-saturation was conducted by pressurizing the flow cell to 4000 psi at 125°C for at least 2 weeks with the laboratory oil. After this time period, the cell was closed off to maintain the high pressure, and the correct connections were made to the accumulator filled with the injection gas. This was done because depressurizing the system would cause some, if not all, of the oil to flow back out of the sample. Unfortunately, doing this meant there was no way to measure the mass of the shale sample after re-saturation.

Starting the Experiment

The first step of experimentation was recording the mass and dimensions of the shale sample, then loading the sample into the flow cell (unless re-saturating was included in the procedures). Due to the high pressures and temperatures in these experiments, the setup was then leak-tested. This was done by first setting the BPR to a pressure significantly greater than 4000 psi in order to ensure there will be no flow out of the system. After setting the BPR, leak-testing was started by closing all valves downstream of the accumulator, and opening them one-by-one, starting with the valve closest to the accumulator. When each valve was opened, the pump volume was closely observed to ensure that there was no leak. After all valves had been opened and all leaks had been remediated, the oven could then be turned on and soaking could begin. For safety reasons, the valve between the flow cell and the BPR was closed during soaking in order to ensure that no gas could exit the system unexpectedly. In this work, the soaking time was approximately 24 hours.

Running a Production Cycle

As described earlier, the huff ‘n’ puff process involves a period of soaking, where the injected gas was allowed ample time to mix with the reservoir oil, followed by a period of production, where the pressure was decreased and the gas-oil mixture was allowed to

flow out. When the time came to run a production cycle, the first thing that was done was fill the liquid collection vessel with toluene and record the volume. After this, the valve between the accumulator and flow cell was closed and the valve between the flow cell and the BPR was opened. At this time, it was important to note the pump volume, which will be used later. The BPR, which is controlled by a syringe pump filled with nitrogen, could then be set to a specific flowrate that allows for the pressure to be drawn down slowly to the desired final pressure. During this time, bubbles should be observed in the toluene, signaling the gas-oil mixture was indeed flowing out of the system.

Once the desired back pressure is reached and the bubbling stops, the valve between the flow cell and BPR was closed, and the BPR pressurized back up to a pressure just below 4000 psi. At this point, the production phase is essentially over, but the system must be "flushed" in order to make sure that no gas-oil mixture is stuck in the flow cell. To do this, the valve between the accumulator and the flow cell was opened, at which time the pump volume would start going down (meaning the flow cell was getting re-pressurized back up to 4000 psi). Once the volume steadies, the valve between the flow cell and BPR was slowly opened, allowing flow out of the system. Once the pump volume had dropped over 50 mL (approximate volume of the flow cell plus all dead volumes) from the level it was at before the production cycle, then the system had been successfully flushed and was then ready to either start another soaking cycle or end the experiment.

3.3.2 Post-Experimental Analysis

Shale samples of nanodarcy-range permeability cannot be tested by conventional coreflooding techniques. Due to the low injectivity, shale samples used in these tests need to be cut into very small core plugs. With these small sample sizes come incredibly small pore volumes. It is therefore impossible to recover and accurately measure oil volumes in

a graduated cylinder, as shown in the results of this work along with other works like Yu and Sheng (2016). In order to accurately quantify oil recovery, effluent was collected in a toluene vial so that it could be analyzed via gas chromatography. On average, the amount of toluene used in the collection process was about 7 mL. This allowed for oil concentrations on the order of 0.5 vol%.

Simulated Distillation (SimDis) was the standardized gas chromatographic method used in the analysis portion of these experiments. This method models the distillation curve of a hydrocarbon mixture and converts retention time to boiling point. SimDis is the method of choice for the self-consistent analysis of petroleum processes and products (ASTM D2887-97a). This is done by injecting a small fluid sample into the GC column, which then heats up according to the SimDis process. As heating occurs, components of the fluid vaporize and are carried to the FID with the carrier gas (helium). Retention time (RT) is then measured. Longer RTs correspond to heavier components with higher boiling points. The results of a GC run are given in graphs like the one shown in Figure 3.6, where the x axis is RT and the y axis is the signal strength. The area under the curve (AUC) for a specific component is not necessarily proportional to the concentration of the component. However, in these experiments it was shown that AUC could be used as a good approximation for calculating how much oil was present in the solutions. In these experiments, the oil recovered was solubilized in toluene, which has a very low RT (~0.1 min) and is therefore easily identifiable compared to the components of the crude oil.

In addition to effluent analysis, the core samples were also analyzed. In earlier experiments, only mass measurements of the shale samples before and after experimentation were used to quantify recovery. However, these measurements come with high levels of uncertainty due to reasons like adsorption, density changes, and precision of equipment. In later experiments, it was proposed to use the same methods as described in

the Solvent Extraction subsection of Section 3.1.2. This offered a way of comparing how the core sample fluid saturations changed from pre- to post-experimentation with much less uncertainty. NMR analysis was also used in several experiments, but was not able to accurately depict any changes in fluid saturations. The results will be shown in Chapter 4 for further discussion.

CHAPTER 4: EXPERIMENTAL RESULTS AND DISCUSSION

A total of five oil recovery experiments were conducted in this body of work: three with the recycled gas and two with pure propane, which is expected to perform better than recycled gas, but is also more expensive. Table 4.1 shows a summary of all results obtained from the experiments. These results will be discussed in greater detail in the following sections.

Table 4.1: Summary of all experimental results.

Experiment	Gas	Temperature (^{0}F)	Soaking Pressure (psi)	Production Pressure (psi)	Surface Area (cm^2)	24-hr Recovery (% OOIP)	48-hr Recovery (% OOIP)
1	HC Gas	257	4000	2000	41.73	N/A	15%
2	HC Gas	257	4000	2000	35.68	N/A	14%
3	HC Gas	257	4000	2000	85.42	N/A	49%
4	Propane	257	2000	0	40.54	12%*	67%
5	Propane	257	1000	0	39.32	55%	N/A

*Low recovery is likely due to experimental error, which will be explained later.

4.1 Recycled Gas Experiments

The first three experiments conducted in this work were all done using the recycled hydrocarbon gas, which was characterized in Section 3.1.1, as the injection fluid. All of these experiments were carried out at 125^{o}C, with injection/soaking at 4000 psi and production at 2000 psi. These pressures were chosen because 4000 psi was assumed to be above MMP and 2000 psi was assumed to be below MMP, meaning the oil would come out of solution during production therefore lowering. According to Sanchez-Rivera (2014), production pressures below MMP outperform production pressures above MMP even with the reduced oil relative permeability solely because of larger drawdown. As stated earlier, the volume of recoverable oil in these experiments is often less than 1 mL, making it

impossible to accurately measure the oil with a graduated cylinder. Therefore, oil recovery was measured by analyzing the mass change of each shale sample before and after experimentation. These experiments were also done under artificially saturated conditions, meaning that the samples were re-saturated with the laboratory oil before experimentation. As stated in Chapter 3, this was done to better replicate the in-situ reservoir conditions, but was also very time consuming and added uncertainty to the results. After experimentation, solvent extraction was conducted on the shale samples, but the liquids were not analyzed with GC. Instead, the crushed shale was dried in a vacuum oven, and the final mass was measured. This step was done in order to quantify any residual oil that was not recovered during the experiments. Table 4.2 shows the mass changes for Experiments 1-3. The saturations were calculated using Equations 4.1 and 4.2:

$$S_{oi} = \frac{m_i - m_{se}/\rho_o}{V_b \varphi} \quad \text{(Eq. 4.1)}$$

$$S_o = \frac{m_f - m_{se}/\rho_o}{V_b \varphi} \quad \text{(Eq. 4.2).}$$

The methods used for these three experiments are very straightforward, but do include quite a few assumptions, such as that re-saturation did not significantly alter the initial mass, no recycled gas was left in the sample after the experiment, and the solvent extraction process recovers all remaining oil after the experiment. Also, because only masses were used in these calculations, recovery could not be quantified after the first production cycle.

Experiments 1 and 2 show an average recovery of 14.5% and Experiment 3 resulted in 49% recovery. This large discrepancy can be explained by the difference in surface areas between the two sets of experiments. Experiments 1 and 2 were conducted with the regular 1” diameter and 1.25” length core plugs, while Experiment 3 was conducted with a core plug of similar size but fractured several times in the direction parallel to the bedding plane.

These results show that there is a strong correlation between huff n' puff performance and surface area, which is a well-known principle and is the basis for hydraulically fracturing unconventional reservoirs. One additional cycle was also conducted for these experiments using a longer soaking time (at least one week) after the first two cycles, but no additional oil was recovered in any of the cases. This points to two key conclusions: that oil recovery is occurring quite rapidly during these experiments and that soaking time does not significantly affect recovery. As Hawthorne et al. (2013) and Sun et al. (2016) hypothesize, diffusion is a significant recovery mechanism in lab-scale experiments, but it occurs very slowly. Therefore, it is likely that convective mixing still dominates the effects brought on by diffusion. This could be due to the fact that the production phase not carried out for a long enough period of time (approximately 4 hours, on average). More experiments must be conducted at different pressures with different production times using more advanced equipment in order to learn more about how oil is recovered during lab-scale huff n' puff.

Table 4.2: Mass and saturation changes for the recycled gas experiments (Experiments 1-3).

Experiment	Initial Mass (g)	Final Mass (g)	Mass After Solvent Extraction (g)	S_{oi}	S_o
1	41.877	41.793	41.323	0.88	0.75
2	31.522	31.460	31.085	0.80	0.69
3	25.431	25.256	25.072	0.83	0.42

4.2 Propane Experiments

Experiments 4 and 5 were conducted using pure propane as the injection gas. These experiments were meant to be used as comparison for the recycled gas experiments, since it is believed that intermediate components such as ethane, propane, and butane are

important for good performance in huff n' puff operations (Fragoso et al, 2015). Additionally, another concern with the recycled gas experiments was the saturation process. It was known because of the sample analysis done in Chapter 3 that there was some in-situ oil saturation left in the samples. Therefore, further saturating the samples with the laboratory oil made it unclear what oil was being recovered, and how these oils differed from one another. As a result, Experiments 4 and 5 were conducted with "as-received" shale samples using improved methodology and equipment. Instead of using the changes in mass to calculate oil recovery, gas chromatography (GC) was used to measure oil concentrations in the effluent, which was bubbled into an aliquot of toluene, and in the shale samples after experimentation. This new methodology allowed for increased accuracy in the measurement of oil recovery, and also decreased experimentation time because re-saturation was no longer necessary.

Before starting the experiments, it was important to characterize the GC response to the oil being solubilized in toluene. Therefore, a set of standard solutions containing known volumetric concentrations of the lab oil solubilized in toluene was created in order to be used as benchmarks for the experimental results. Figure 4.1 shows the GC results for the standard solutions used in these experiments. Qualitatively, there are several key takeaways from these results. First, it is important to note that the toluene peak is clearly present in all responses (except for the response for pure oil). Secondly, it is apparent that as vol% of oil increases, % AUC (area under curve) decreases in the toluene peak. For example, the 0.1 vol% response in Figure 4.1 is on average the lowest in the RT (retention time) range where oil components are found, and the pure lab oil response is by far the highest. Figure 4.2 shows the linear relationship between % AUC of the toluene peak and vol% of oil in these standardized solutions. This is a very important finding, both qualitatively and quantitatively, but must be used with caution. Comparing Figure 4.1 to

Figure 3.10 shows that the GC response of the laboratory oil is slightly different than that of the in-situ oil. This means that although it is safe to assume that the in-situ oil will behave in a similarly linear fashion, the exact slope and intercept of the line cannot be directly applied to Experiments 4 and 5. Therefore, is it assumed that % AUC of the toluene peak is equal to vol% of toluene, and hence vol% of oil is equal to 100 minus the % AUC of the toluene peak.

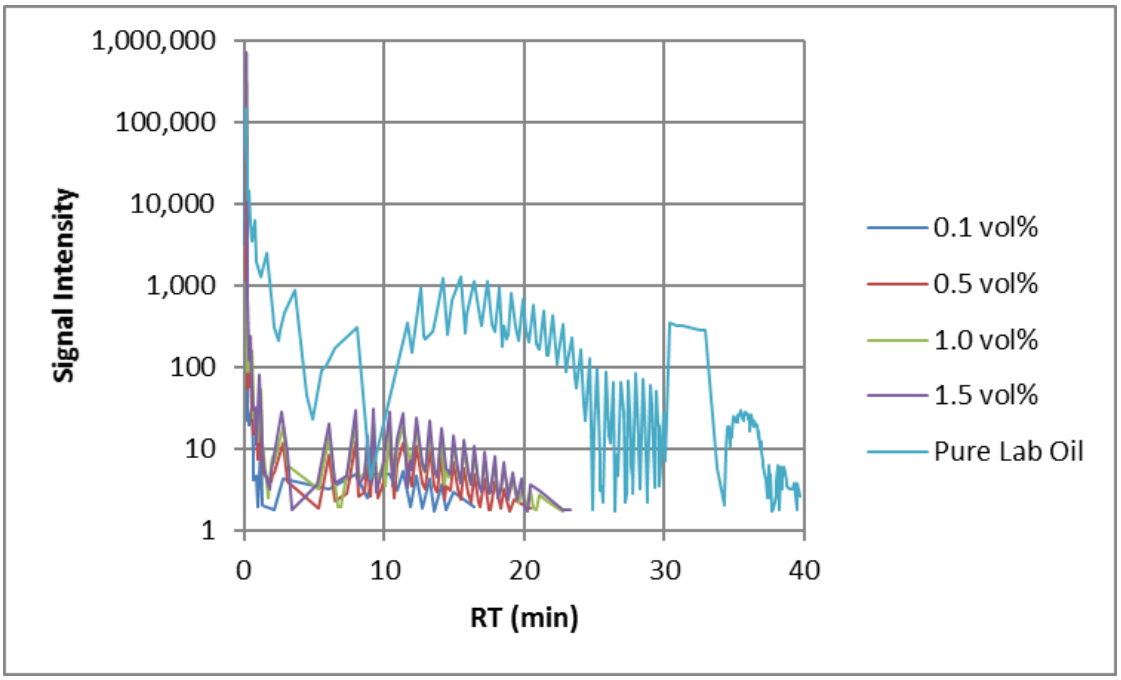

Figure 4.1: GC results for standardized solutions of lab oil in toluene.

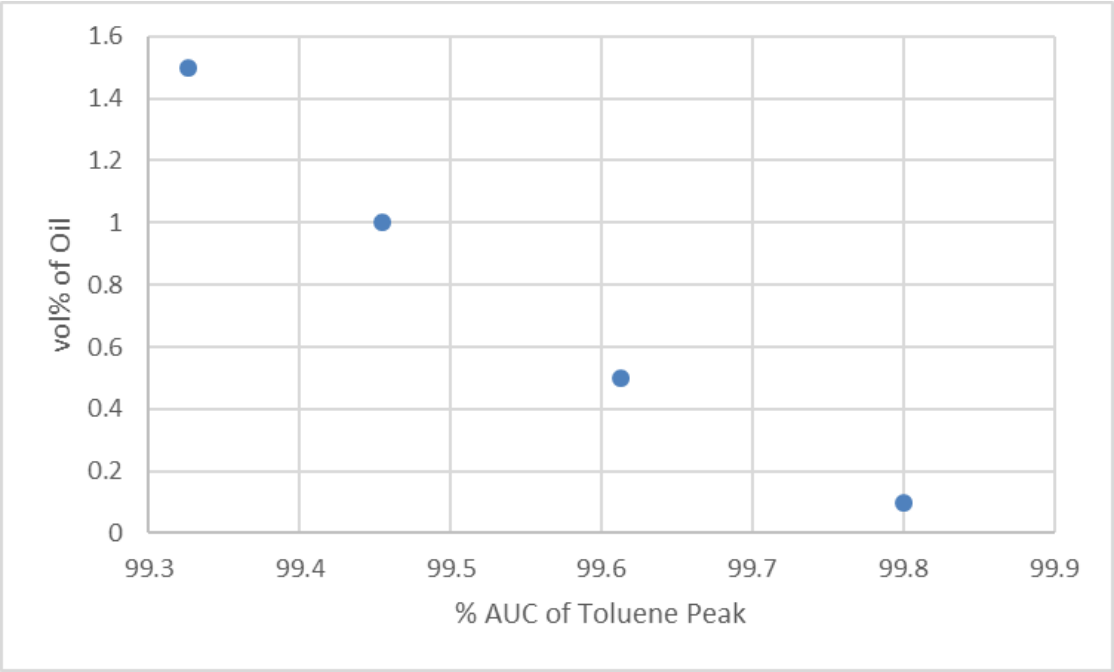

Figure 4.2: Linear relationship between % AUC of the toluene peak and vol% of oil in the standardized solutions.

Table 4.1 shows that the propane experiments significantly outperformed the recycled gas experiments. Experiment 4 had a final oil recovery of 67%, and Experiment 5 had a final recovery of 55% (after 24 hours). Experiment 5 was cut short due to malfunction in the experimental equipment, however good results were still obtained for the first huff n' puff cycle. With the improved methodology described above, recovery was able to be observed after each cycle, as in Experiment 4. Unfortunately, though, the results obtained for the first cycle in Experiment 4 do not seem reliable. It is thought that not all oil produced during the first cycle came out of the tubing and into the collection vessel, and instead came out with the oil produced in the second cycle. So, although the recovery for the first cycle is lower than expected, the final recovery is still considered to be accurate. To ensure this problem didn't happen again, it was proposed to flush the system with

nitrogen after every production cycle in order to ensure nothing had accumulated in the tubing.

Figure 4.3 shows the GC results of the effluent in Experiment 4. As shown, cycle 2 clearly extracted more oil than cycle 1. Using the calculation method described previously, approximately 0.03 mL of oil was recovered during the first cycle, and 0.15 mL was recovered during the second cycle. Moreover, the right-hand plot in Figure 4.3 is zoomed in to show the oil portion of the Experiment 4 results compared to the standardized solutions. As shown, one can see that the 48-hour effluent contained between 0.1 and 0.5 vol% of oil. This qualitative observation is in agreeance with the calculations, which show that the 48-hour effluent effluent contained about 0.26 vol% of oil. The shale sample itself was also analyzed after the experiment to investigate how much residual oil was left. Figure 4.4 shows the results of this test along with the initial GC results conducted on an "as received" shale sample (see Figure 3.10). This test was done using the exact same procedures as the initial analysis (see Section 3.1.2). As shown, there is a significant drop in the oil portion of the GC results. Calculations show that the final oil saturation of the sample in Experiment 4 was approximately 0.27, compared to an approximate initial saturation of 0.45.

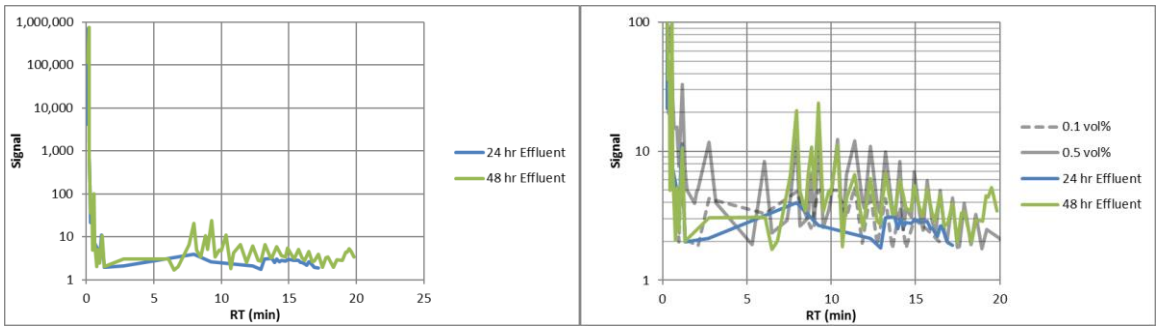

Figure 4.3: GC results for effluent after 24 and 48 hours in Experiment 4. Left plot is the complete results, while the right plot is zoomed in to display the oil portion of the results, which shows qualitatively how much oil was in the effluent compared to the standard solutions.

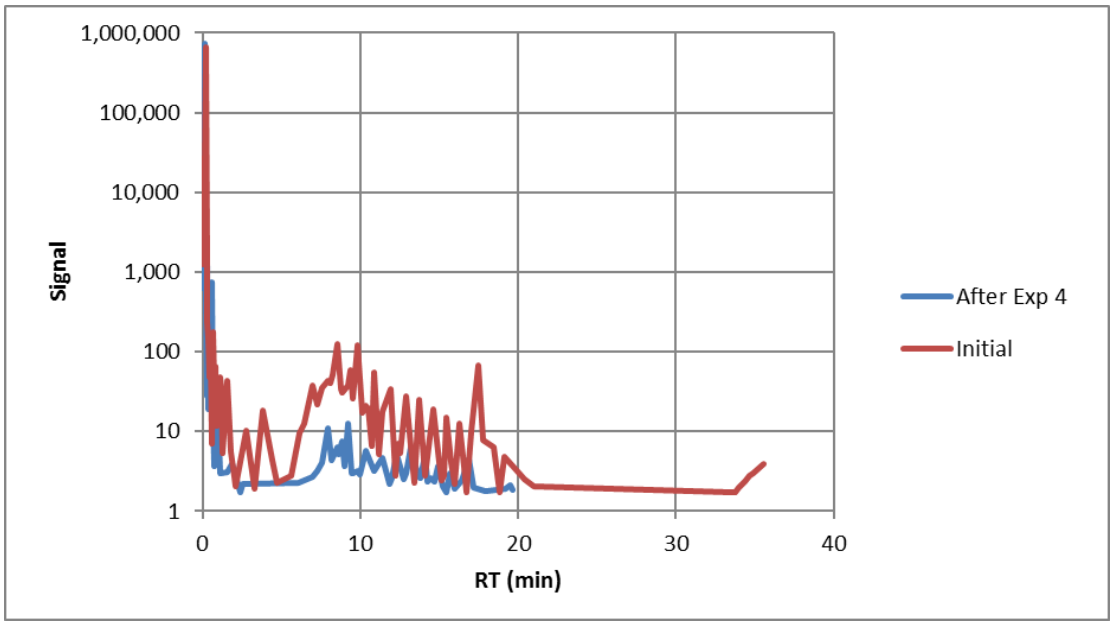

Figure 4.4: GC results for the toluene extraction in Experiment 4.

Experiment 5 was carried out like Experiment 4, but the soaking was done at 1000 psi instead of 2000 psi. This led to slightly lower recovery, but still higher than the recycled gas experiments, which were all carried out at 4000 psi. However, the 24-hour recovery was higher in Experiment 5 than Experiment 4, although exactly how much higher is not well-known because of the possible error in Experiment 4. Figure 4.5 shows the effluent

results of Experiment 5 in the same manner as Figure 4.3. Approximately 0.15 mL of oil was recovered, which corresponds with approximately 55% recovery. Furthermore, the right plot in Figure 4.5 shows the oil portion of the Experiment 5 results compared to the 1.5 vol% standardized solution. It shows that the effluent has a slightly higher concentration of oil than the standardized solution. This aligns well with the calculations, which show an oil concentration of approximately 1.7 vol%.

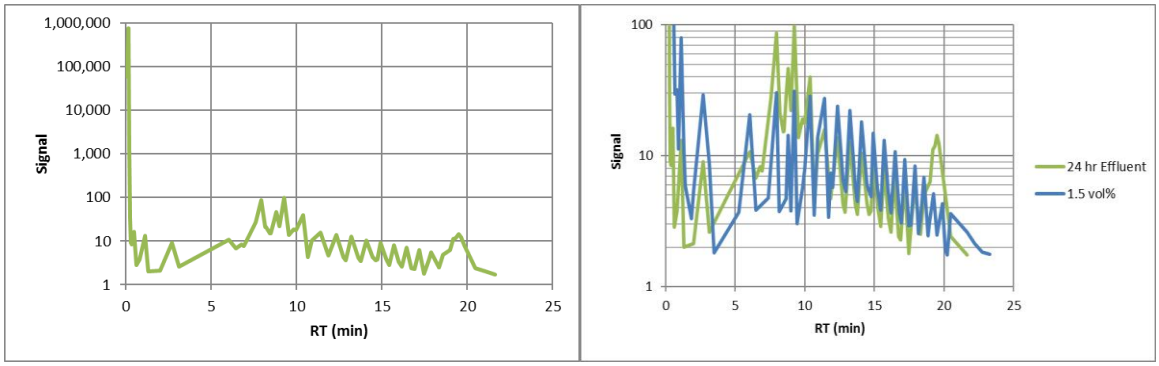

Figure 4.5: GC results for effluent collected after 24 hours in Experiment 5. Left plot is the complete results, while the right plot is zoomed in to display the oil portion of the results, which shows qualitatively how much oil was in the effluent compared to the standard solutions.

4.3 Discussion of Results

In the recycled gas experiments, recovery was found to be approximately 15% after two huff n' puff cycles for un-fractured samples, and 49% for fractured samples. Furthermore, the experiments were allowed to run for an extra cycle where the soaking time was one week, but no additional oil was recovered. In the propane experiments, recovery was significantly higher than the recycled gas experiments despite having lower soaking pressures. Additionally, Experiment 4 recovered slightly more oil than Experiment

5, but 24-hour recoveries showed Experiment 5 performing better than Experiment 4. There are several key questions that must be answered about these results. First, why did the propane experiments outperform the recycled gas experiments? This is likely due to two reasons. The first being that propane is more miscible with the oil than the recycled gas, even at the lower pressures. Enhanced miscibility leads to better oil recovery, whether it be because of oil swelling, oil viscosity reduction, interfacial tension reduction, or the formation of a robust miscible phase. From these experiments, it was not possible to observe the effects of diffusion, but it is not clear whether or not it plays a significant role in mixing when compared to convection. The second reason is that the propane experiments were produced at a much lower pressure than the recycled gas experiments (atmospheric pressure compared to 2000 psi in the recycled gas experiments). This means that the ratio between soaking pressure and production pressure is a significant factor in recovering oil via huff n' puff. The second question that must be answered is why there was no additional oil recovered in the extra huff n' puff cycle of the recycled gas experiments. This could possibly be due to the fact that diffusion, which is much slower than the other mass transfer phenomena, is not significantly affecting oil recovery, and hence performance is not significantly dependent on soaking time. Another reason could be because of channeling within the sample. In order to make more accurate conclusions about these findings, the experiments done in this work will be numerically modeled. These results will be discussed in Chapter 5.

CHAPTER 5: COMPOSITIONAL MODELING APPROACH

This chapter studies the complete process of numerically modeling the huff n' puff recovery technique in a LRS reservoir. Specifically, it will be attempted to replicate the lab-scale experiments done in Chapter 4 as closely as possible in order to learn more about the complex recovery mechanisms at play. Then, a field-scale study will be done incorporating a live-oil fluid model in order to compare results. These models were all built using the GEM simulator, which is made by Computer Modeling Group (CMG). GEM is CMG's advanced general equation-of-state compositional simulator, which is necessary for complex gas injection EOR processes such as the one studied in this work. The model built in this study was composed of two main parts: fluid characterization and computational domain. Sections 5.1 and 5.2 discuss these parts in detail. Section 5.3 discusses the results of the lab-scale simulations, and Section 5.4 gives a brief summary of some field-scale models that were built.

5.1 Fluid Characterization

Accurate fluid characterization is vital for reservoir modeling in a compositional simulator. Normally, the assembly of an accurate fluid model involves the collection of experimental fluid data, selecting an EOS, and tuning the EOS to match the experimental data. However, in this work the fluid model used was already tuned for this specific reservoir, so no further tuning was needed. In this work, the fluid model was generated using CMG's fluid modeling software WinProp (CMG, 2015). The oil used in these simulations was modeled to be identical to the dead laboratory oil used in the experimental portion of this work. Unfortunately, the model provided was tuned for the live reservoir oil, so the dead oil composition had to be created from scratch. This was calculated using

the QNSS/Newton flash method, in which the live oil was flashed at atmospheric conditions. The Peng-Robinson (1978) EOS was used with Peneloux constant volume shift correction. Viscosity was calculated using the modified Pedersen (1987) model, which shows improved results for mixture viscosities up to approximately 10 cP (CMG, 2015). The oil and gas diffusion coefficients were calculated using the Sigmund correlation.

Components were lumped into 13 pseudocomponents based on the lumping scheme suggested by Zhu et al. (2015). Table 5.1 shows the lumping scheme and composition of the oil. Specific gravity, boiling temperature, critical PVT, acentric factor, and molecular weight are all important parameters for tuning the fluid model. Tables 5.2 shows these values for each pseudocomponent. Refer to Figures 3.1-3.3 for data regarding viscosity, density, and phase behavior of the oil, which all agree well with experimental data provided for the target reservoir. Because of the low density of the oil, there were initially some problems with phase identification in the fluid model. To fix these problems, the model was altered to identify phases based on the calculated pseudo-critical temperature of the mixture in each block rather than calculated fluid density. The Li mixing rule given below was used for calculating the critical temperature:

$$T_{c,mix} = \frac{\sum_i z_i v_{c,i} T_{c,i}}{\sum_i z_i v_{c,i}} \qquad \text{(Eq, 5.1.1)}$$

where z_i is the global mole fraction of component i and $T_{c,i}$ and $v_{c,i}$ are the critical temperature and volume of component i (CMG, 2015). This allowed for much more accurate phase identification, which is crucial in huff n' puff as there is a great deal of phase change throughout the process. Another important parameter for the fluid model is the MMP. This was calculated using the cell-to-cell method for oil-recycled gas and oil-propane systems. Table 5.3 shows the results of these calculations, which confirm that both experimental cases were conducted above MMP during injection/soaking and below it during production.

Table 5.1: Composition of the laboratory oil at room conditions.

Pseudocomponent Composition (mol%)												
N2	**CO2**	**C1**	**C2**	**C3**	**C4**	**C5**	**C6**	**C7-9**	**C10-13**	**C14-17**	**C18-22**	**C23-79**
0	0.15	0.37	0.43	0.82	1.68	3.23	5.34	31.15	27.55	14.27	8.54	6.61

Table 5.2: Important parameters for each pseudocomponent used in the fluid model.

Pseudo-component	Specific Gravity	T_b (°F)	P_c (psi)	V_c (L/mol)	T_c (°F)	Acentric Factor	Mol. Wt.
N2	0.809	-1036.30	492.31	0.090	-232.51	0.040	28.01
CO2	0.818	-656.25	1069.86	0.094	87.89	0.225	44.01
C1	0.300	-925.17	667.19	0.099	-116.59	0.008	16.04
C2	0.356	-689.30	708.34	0.148	90.05	0.098	30.07
C3	0.507	-538.31	615.76	0.203	205.97	0.152	44.10
C4	0.577	-416.50	543.48	0.258	295.05	0.187	58.12
C5	0.628	-298.72	490.15	0.305	377.27	0.239	72.15
C6	0.690	-195.20	477.03	0.344	453.83	0.275	86.00
C7-9	0.747	-24.88	428.77	0.419	563.51	0.346	106.63
C10-13	0.772	204.97	317.44	0.602	686.45	0.505	151.43
C14-17	0.809	409.80	253.84	0.776	804.25	0.682	210.52
C18-22	0.864	620.97	225.24	0.906	927.28	0.835	272.56
C23-79	0.981	1030.42	200.03	1.094	1149.28	1.030	395.20

Table 5.3: MCM and FCM pressures for recycled gas and propane with the lab oil.

Injection Gas	MMP (psi)	FCM (psi)
Recycled Gas	3,720	4,380
Propane	775	1,000

5.2 Computational Domain

During the experiments, the core samples were unconfined within the flow cell as a way of mimicking the presence of a high-permeability fracture system. Therefore, a Cartesian grid was selected in order to easily incorporate the high-permeability "fracture" zone and the low-permeability matrix. In order to save computational time, a 2D model was chosen. The total dimensions of the model were 6 in x 4 in x 1 in, with the actual sample having dimensions of 3 in x 2 in x 1in. The sample portion of the model was finely discretized into 800 grid blocks, and the fracture contained 352 grid blocks. Further discretization did not significantly affect results, but did increase computational time. Figure 5.1 shows a view of the domain from the x-y point-of-view.

In these lab-scale models, the matrix was assumed to be homogenous and isotropic. Based on data mentioned in Chapter 3, the porosity was set to 7% and permeability was set to 500 nD in the matrix. For the fracture region, the porosity and permeability were 50% and 5 D, respectively. Initially, the core was saturated with 80% oil and 20% immobile water, and the fracture was saturated with 80% injection gas and 20% immobile water. Adsorption and desorption of hydrocarbons onto the rock matrix were not accounted for in these models. Like the experiments, the system was initialized at a low pressure (100 psi), and then pressurized by injecting the gas at a reasonable flow rate (less than 100 mL/min) up to the desired soaking pressure. The relative permeability curves were adapted from Honarpour et al. (2012), where conventional Corey-type curves are used in the matrix and straight-line curves are used in the high-permeability fractures. The accuracy of this method is highly unknown, though, due to the difficulty of fractional flow measurement in nanodarcy rocks.

The model was set to simulate two huff n' puff cycles. The system is first pressurized up to the desired soaking pressure by injecting the gas for 6 hours, then 24 hours of soaking occurs, and finally 6 hours of production is completed at the desired production pressure. After that, one more cycle is conducted. Two sets of injection and production wells were created and perforated identically so that the injection gas could access both sides of the matrix easily, and the oil would not get trapped in the fracture system. Table 5.4 summarizes the model inputs below.

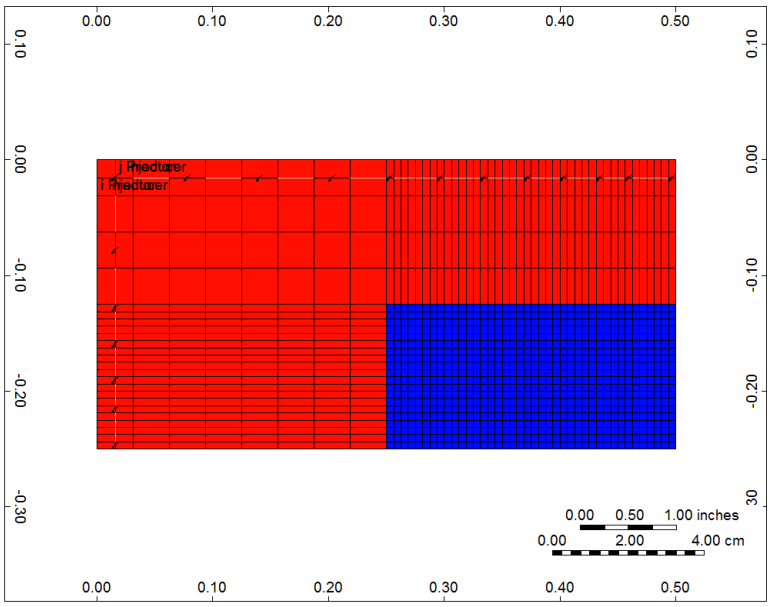

Figure 5.1: Cartesian grid of the core sample (blue) surrounded on two sides by the high-permeability fracture zone (red).

Table 5.4: Summary of lab-scale model inputs.

Model Inputs	Value
Porosity, matrix	7%
Porosity, fracture	50%
Permeability, matrix	500 nD
Permeability, fracture	5 D
Initial water saturation	20%
Reservoir temperature	257 °F
Initialization pressure	60 psi
Injection pressure*	4000 psi
Production pressure*	2000 psi
Reservoir depth	11,000 ft
Injection period	0.25 days
Production period	0.25 days
Soaking period	1 day
* default values	

5.3 Results and Discussion

The lab-scale numerical simulations had two primary goals: to verify the experimental results found in Chapter 4 and to also study the effect that production and injection pressures have on huff n' puff performance. The first case that was examined was meant to replicate Experiments 1-3 (i.e. recycled gas used as injection fluid and default inputs in Table 5.4 were used). Figure 5.2 shows the oil recovery results for this model. The original oil in place (OOIP) was 3.8 mL in this case, which means that the first huff n' puff cycle recovered 0.30 mL and the second cycle recovered an additional 0.11 mL. These numbers agree well with the results shown in Experiments 1-3, which also had total oil

recoveries in the range of less than 1 mL. The recovery percentages are slightly lower than what was seen in the experiments, but this is expected considering the domain of the model. Only two sides of the sample are exposed to the injection and production wells, meaning that the sweep efficiency of the model is roughly half of what it should be theoretically. With this being considered, the recovery results also agree quite well with what was seen in Experiments 1-3. Figure 5.3 shows the average pressure of the sample over the entire duration of the model. Due to the small size of the model, pressure propagates quickly through the domain especially in the first cycle. However, during the second cycle there is a significant portion of gas trapped in the shale, which significantly slows the increase in pressure due to injection. This is the reason why the desired soaking pressure was not achieved, as shown in the plot, and is likely a contributing factor to lower recovery after the second cycle.

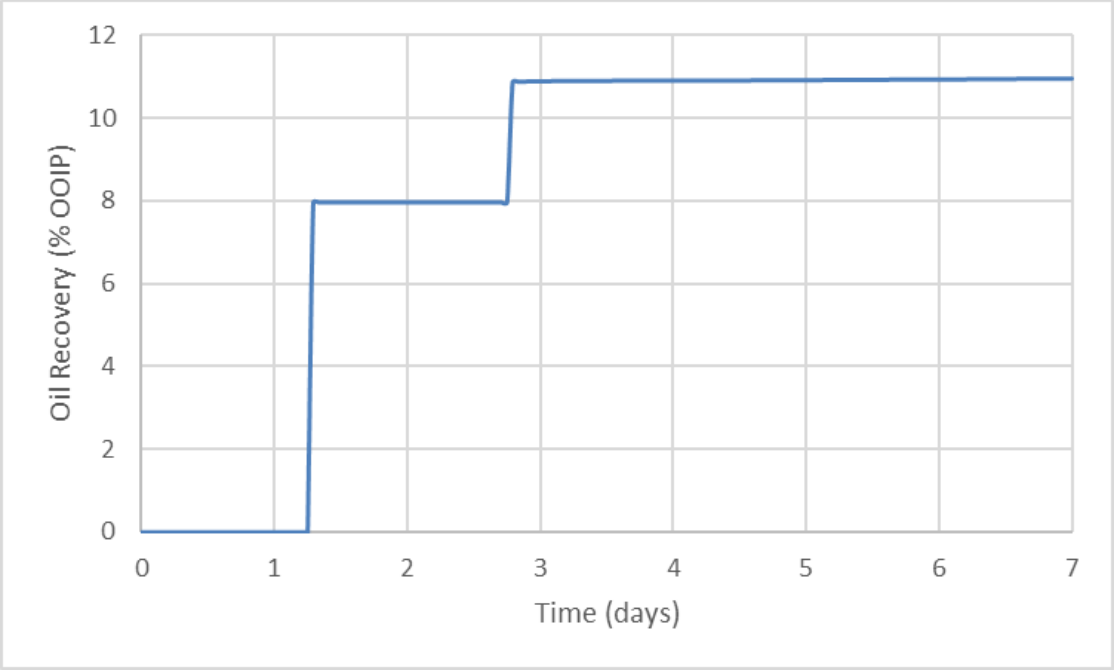

Figure 5.2: Oil recovery for the base case lab-scale model.

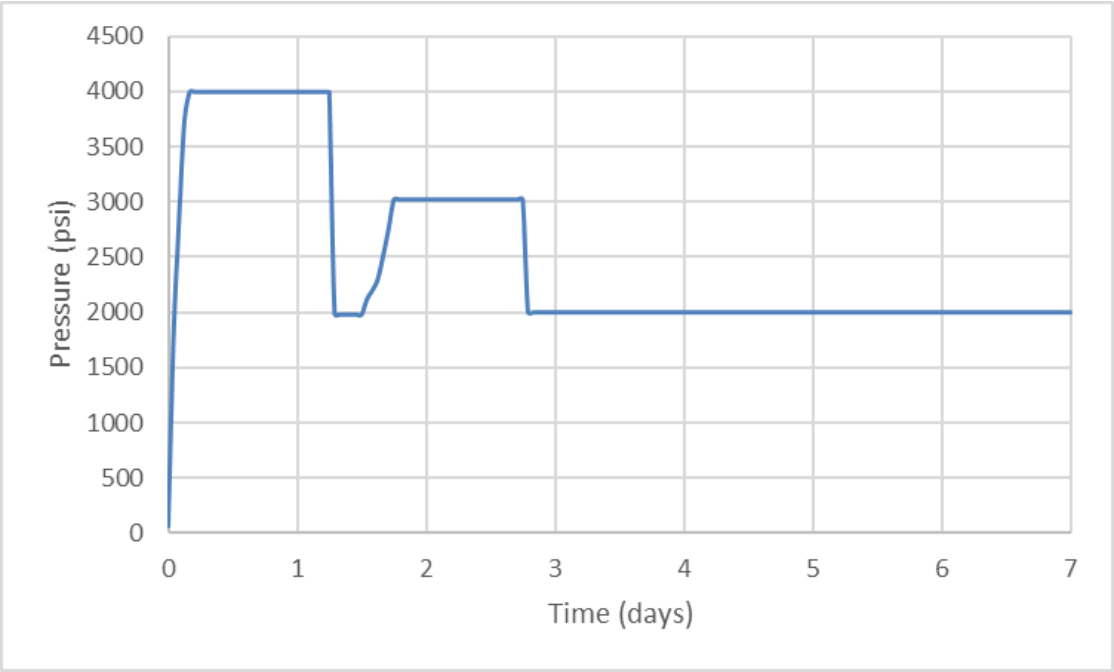

Figure 5.3: Pressure of the base case lab-scale model.

Along with this base case model, there were also two other models that were ran to further investigate the recovery mechanisms at play during the lab-scale experiments: one with a reduced production pressure (1000 psi) and one with an elevated injection pressure (5000 psi). There have been several works whose aim was to investigate the effects of production and injection/soaking pressures during huff n' puff operations (Sun et al, 2016; Hawthorne et al, 2013; Zhu et al, 2015). It has been hypothesized that injection pressure is an important parameter in huff n' puff treatments, but the reason why and if it translates to the lab scale is still unclear. Figure 5.4 shows the results of all three cases. This plot shows that the effect of production pressure vastly outweighed the effect that injection pressure or increasing the difference between the two pressures had on performance in these models. In fact, the base case performed slightly better than the 5000 psi injection case, which is likely due to the higher pressure forcing oil deeper into the matrix, making it harder to

recover. Lowering the production pressure to 1000 psi increased incremental recovery by almost 50% when compared to the base case, which used a 2000-psi production pressure.

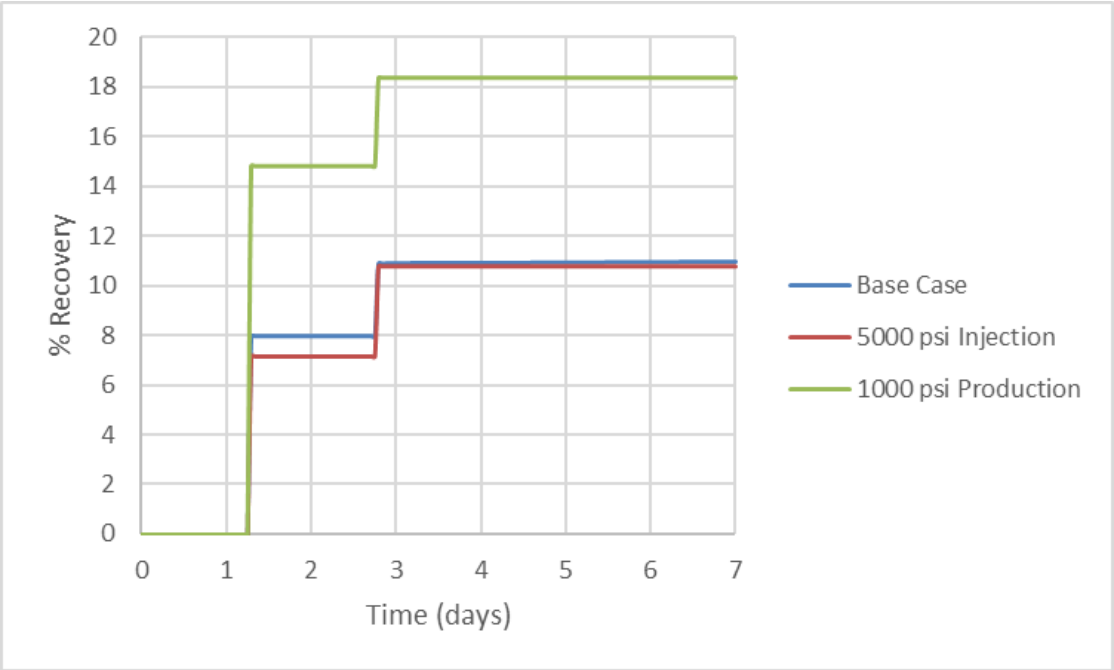

Figure 5.4: Oil recovery for all three lab-scale models.

Figure 5.5 shows the gas saturation and global mole fraction of C1, which is the dominant component in the recycled gas, at the end of the first injection cycle for each of the three cases. As long as injection took place above MMP, it was shown that the gas and oil mixed similarly in all cases regardless of pressure. Because of this, it is hypothesized that sweep efficiency does not play a significant role in performance when compared to the field scale. Higher injection pressure in the field likely enhances performance due to the fact that larger channels of gas will be created and therefore *more* mixing is able to occur. However, this is not the case in lab-scale experimentation because of the small sample size. Results shown in Figure 5.6 show that viscosity reduction does not significantly affect

recovery in these lab-scale models, either. During injection the viscosity decreases as gas solubilizes into the oil, and during production the viscosity increases back to around the initial condition as the gas evolves out of the oil. However, there was no indication that the 1000-psi production case benefitted from lower viscosities because the other two cases, on average, had lower oil viscosities. The small size of the lab scale models allows for all oil to be mixed with the gas quickly and fairly uniformly, minimizing the effect of decreasing viscosity during injection. This differs from larger-scale models, where there are usually large discrepancies between the oil viscosity near a fracture face and the oil viscosity inside the bulk matrix.

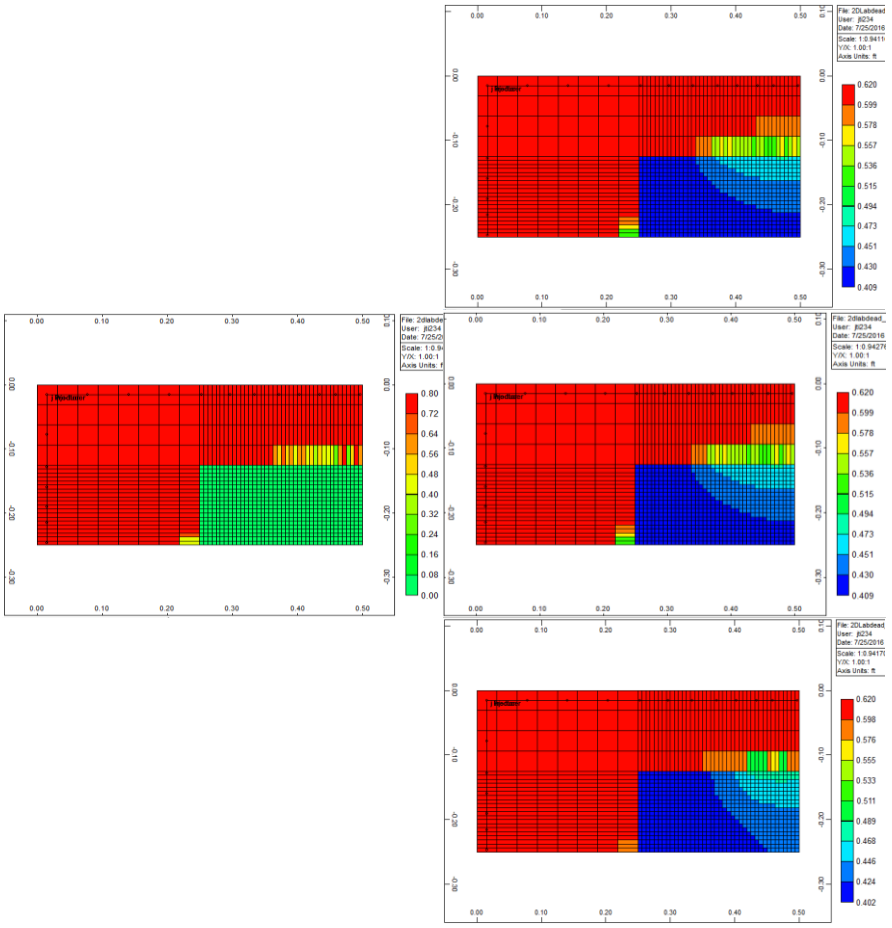

Figure 5.5: gas saturation (left) and global mole fraction of C1 in the base case (top right), 1000 psi production case (middle right), and 5000 psi injection case (bottom right) after the first injection phase.

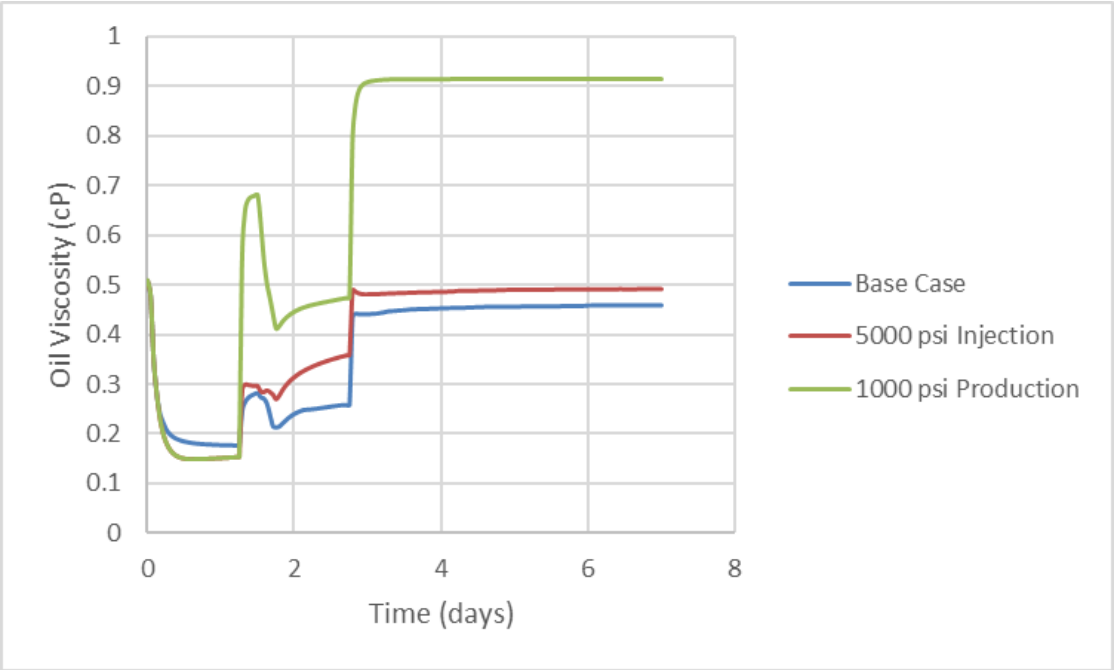

Figure 5.6: Oil viscosity as a function of time for all three lab-scale models.

5.4 Field-Scale Modeling

In addition to the lab-scale models, a field-scale investigation was done in order to better understand how the mechanisms observed in the experiments come into play in reservoir-scale huff n' puff operations.

5.4.1 Fluid Characterization

Besides the difference in size, the most prominent difference between the lab-scale modeling and the field-scale modeling is the fluid model. In the laboratory, dead oil was used because it's much easier to work with and is also safer. However, experiments using dead oil can at times be a poor approximation for what occurs in situ, especially if the oil being studied is light. In the case of this study, the oil is indeed very light, and therefore differs significantly in composition from the dead laboratory oil. In order to maintain consistency, the lumping scheme and parameters were not changed when going to the live

oil model. Table 5.5 shows the composition of the live oil, which contains over 50 mol% of C1 at reservoir conditions. This differs significantly from the laboratory oil, which contains less than 1 mol% of C1. Figure 5.7 is a plot of the P-T diagram for the live oil, which shows that at reservoir temperature the saturation pressure is 4,205 psi. At initial reservoir conditions (7,200 psi and 257°F), the oil viscosity is 0.11 cP and density is 0.50 g/cm^3. The MMP was also recalculated for the live oil using the same method as was used in the dead oil case. Table 5.6 shows the results of these calculations. Compared to the MMP results of the dead oil shown in Section 5.1, the MMP and FCM pressures are slightly higher for the live oil due to the increased amount of light components already solubilized in the oil.

Table 5.5: Composition of the live reservoir oil at initial reservoir conditions.

Pseudocomponent Composition (mol%)												
N2	**CO2**	**C1**	**C2**	**C3**	**C4**	**C5**	**C6**	**C7-9**	**C10-13**	**C14-17**	**C18-22**	**C23-79**
0.07	0.9	58.2	11.6	6.05	4.12	2.69	1.95	5.66	4.26	2.19	1.31	1.02

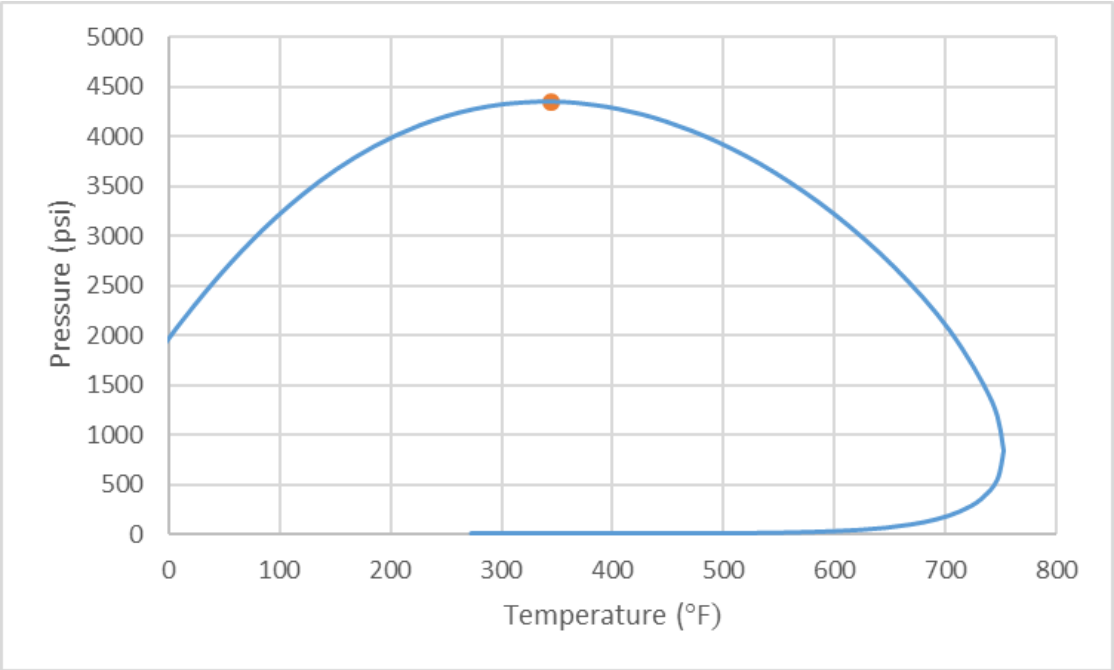

Figure 5.7: P-T diagram for the live oil.

Table 5.6: MMP and FCM pressure for various injection gases with live oil.

Injection Gas	MCM (psi)	FCM (psi)
CO_2	4,313	4,888
Methane	4,338	7,725
Recycled Gas	4,313	4,525
Propane	775	4,170

5.4.2 Computational Domain

A scheme of the Cartesian grid used in this field-scale study is shown in Figure 5.8. This model attempts to simulate the huff n' puff process in a hydraulically fractured reservoir. The domain consists of two half-fracture stages located at the domain boundaries, which are 210 feet long and have a spacing of 200 feet. Natural fractures were also included in this model to better replicate the target reservoir, which is thought to have extensive natural fracture systems and therefore play a crucial role in performance

(Fakcharoenphol et al, 2012). These natural fractures are 10 feet in length and intersect the hydraulic fractures perpendicularly. The domain was also discretized into 15 evenly-sized grid blocks in the z direction in order to study the effects of gravity. A reservoir thickness of 50 feet was used as suggested by Gong et al. (2013).

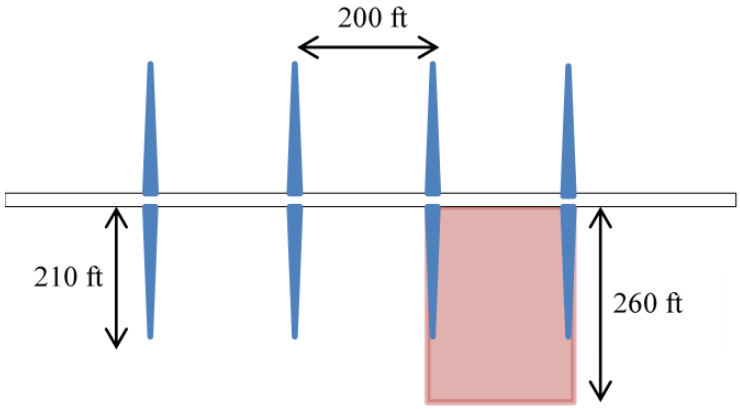

Figure 5.8: Well completion scheme with a horizontal well and intersected hydraulic fractures. The computational domain is shown in red.

A single-porosity model was used for computation. Like the lab-scale model, the matrix was assigned a permeability of 500 nD. The hydraulic fractures and natural fractures have permeabilities of 10 D and 100 mD, respectively. Because the large contrast between permeabilities can lead to numerical instability and long run times, effective fractures were created (Sanchez-Rivera et al, 2015). This was done by simultaneously scaling up the fracture widths and scaling down the fracture permeabilities in order to keep the fracture conductance, which is the product of fracture permeability multiplied by fracture width, constant. This resulted in 5-ft wide hydraulic fractures with a permeability of 10 mD and 6-ft wide natural fractures with a permeability of 0.05 mD. The grid was discretized into 5,400 blocks, with fine gridding around the fractures. Further discretization was not heavily investigated in this study. Figure 5.9 shows the computational domain as rendered by CMG GEM, and Table 5.7 summarizes all model inputs.

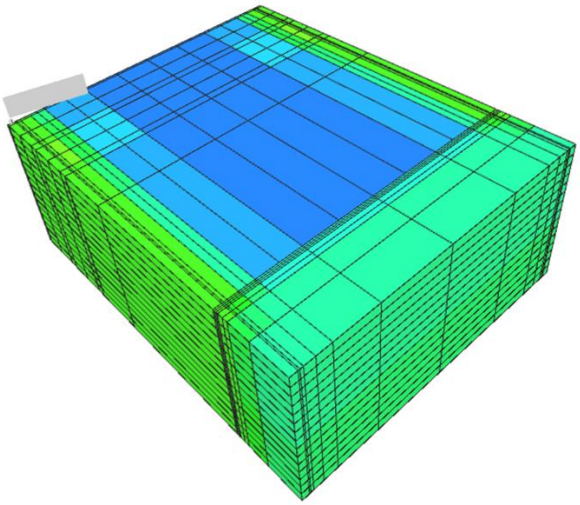

Figure 5.9: Computational domain for the field-scale case. The horizontal well runs along the back boundary with perforations at each fracture (left and right boundaries).

Table 5.7: Summary of model inputs for the field-scale case.

Property	**Value**
Matrix permeability	0.0005 mD
Hydraulic fracture width (real/model)	0.005/5 ft
Hydraulic fracture permeability (real/model)	5000/10 mD
Hydraulic fracture porosity (real/model)	0.43/0.00043
Natural fracture width (real/model)	0.003/6 ft
Natural fracture permeability (real/model)	100/0.05 mD
Natural fracture porosity (real/model)	1.0/0.0005 ft
Hydraulic fracture spacing	200 ft
Initial water saturation	0.2
Initial reservoir pressure	7,200 psi
Injection pressure	7,000 psi
Production pressure	1,000 psi
Reservoir temperature	257°F
Reservoir depth	11,000 ft

5.4.3 Results and Discussion

A base case was conducted in order to simulate the primary production of this reservoir. In order to save computational time, the model was made into a 2D case with only one 50-ft grid block in the z-direction. The reservoir was depleted from the initial reservoir pressure of 7,200 psi to 1,000 psi over the course of 10 years. At that point, the total recovery was 12.76% of the original oil in place (OOIP). However, it was elected to start the huff n' puff operations after 5 years based on the sharp drop in production rate and based on the idea of maintaining some of the initial reservoir pressure. Figures 5.10 and 5.11 show the results of this primary production phase.

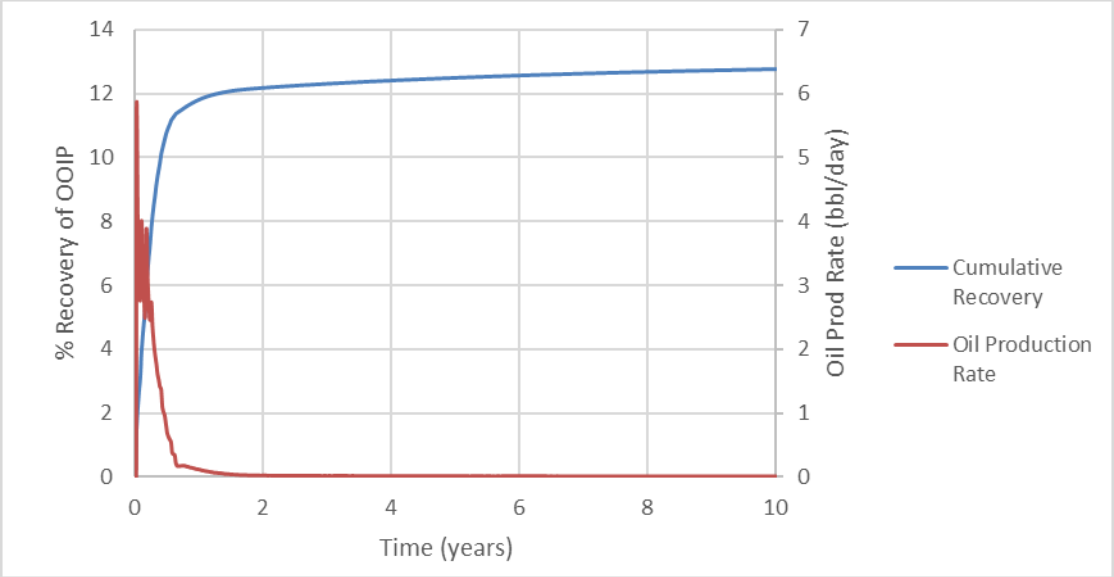

Figure 5.10: Recovery and production results for the primary production phase.

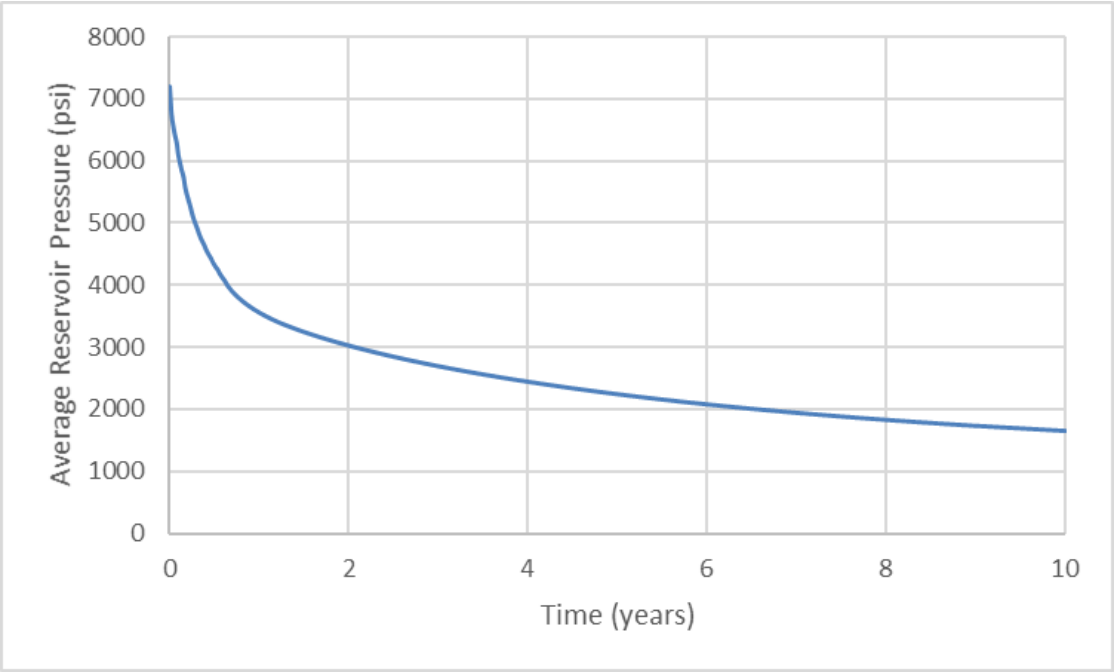

Figure 5.11: Average reservoir pressure during the primary production phase.

After the primary production case was completed, data such as saturations, pressures, and compositions needed to be extracted and implemented into the 3D huff n' puff case. This was done by altering the initial conditions portion of the 3D model. Instead of assigning a constant initial pressure and global composition scheme, a vertical depth-averaged initialization method was used. In this method, 3 regions were specified: the hydraulic fractures, the matrix between the two fractures, and the bulk matrix beyond the fractures. Each region was assigned an average pressure and oil and gas composition based off block data taken from the 2D model at the 5-year mark. This allows the simulator to initialize the saturation of each grid block based on flash calculations carried out at the specified pressure. Figure 5.12 shows the initial saturation conditions of the 3D model at the top, middle, and bottom of the reservoir. Because the reservoir is below saturation pressure, it is highly saturated with gas that this point. The fractures show no oil at all

(pressure is lowest in the fractures) while the matrix shows oil in the lower part of the reservoir due to gravity segregation. These initial conditions agree well with the conditions seen in the 2D model after 5 years of depletion. Figure 5.13 and Table 5.8 show the timing of the huff n' puff process and relevant reservoir data at the start of huff n' puff, respectively.

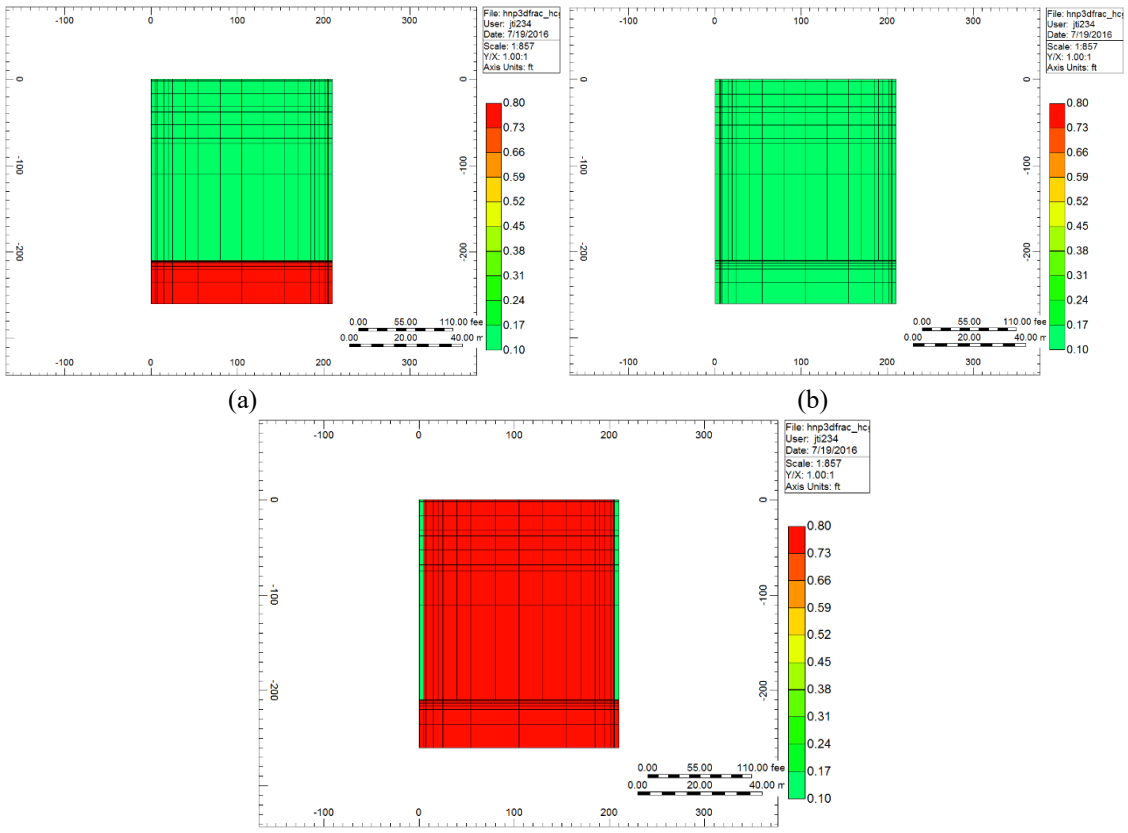

Figure 5.12: Oil saturation of the top (a), middle (b), and bottom (c) of the reservoir at the start of the huff n' puff process.

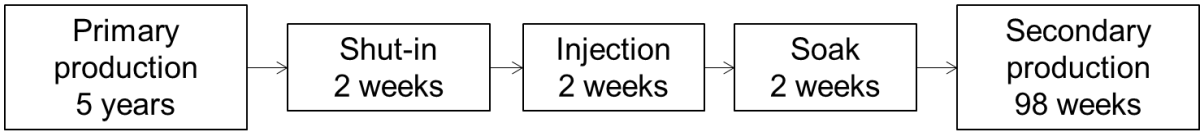

Figure 5.13: Timing scheme of the field-scale huff n' puff process.

Table 5.8: Relevant reservoir data after five years of primary depletion and just before the start of huff n' puff.

Property	Value
OIP	8,005 STB
GIP	14.3 MMSCF
Avg Reservoir Pressure	1,945 psi

The results of the first case are shown in Figure 5.14. This case used the recycled gas as the injection fluid with all of the default inputs found in Table 5.7. The results show 1.5% incremental oil recovery after a single huff n' puff cycle. When compared to the low primary production recovery of 12.5%, this is a significant increase in performance especially when considering the low cost of executing this specific huff n' puff scheme. The gas is readily available from the reservoir, and no other wells need to be drilled as injectors. As Figure 5.14 points out, the average reservoir pressure did not increase high enough to achieve miscibility in the bulk of the reservoir. However, pressures around the fractures were high enough to achieve miscibility as shown in Figure 5.15 (top). Figure 5.15 shows a plot of pressure (top) and viscosity (bottom) vs. time at two different points within the reservoir: one inside a natural fracture and one 90 feet from a hydraulic fracture. These two plots indicate that in-situ conditions vary greatly from the fractures to the bulk matrix and that much of the recovery occurs within several feet from the fractures, therefore emphasizing the fact that more extensive fracturing (and hence, sweep efficiency) leads to better recovery in general. The viscosity plot in Figure 5.15 also points out a key difference between the lab-scale and field-scale models. In these field-scale models, live oil with a

saturation pressure of about 4,300 psi was used. This means that oil was produced below the bubble point and explains why Figure 5.15 shows an increase in oil viscosity of almost 400% when compared to the oil viscosity at initial reservoir conditions. Therefore, as Sanchez-Rivera (2014) and Sun et al. (2016) conclude, gas expansion caused by production below bubble point is a key factor in enhancing performance. The decrease in oil viscosity during injection also plays a key role in recovering oil in this model, but because the viscosity rises quickly and substantially near the fractures ultimate recovery still remains low.

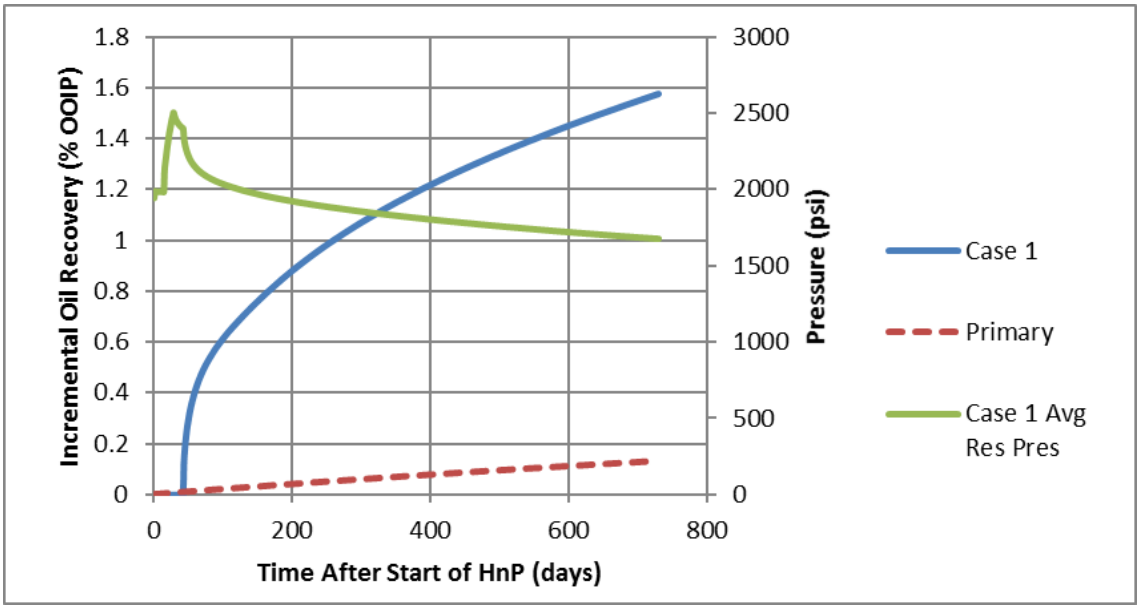

Figure 5.14: Incremental recovery and average reservoir pressure vs. time during one field-scale huff n' puff cycle.

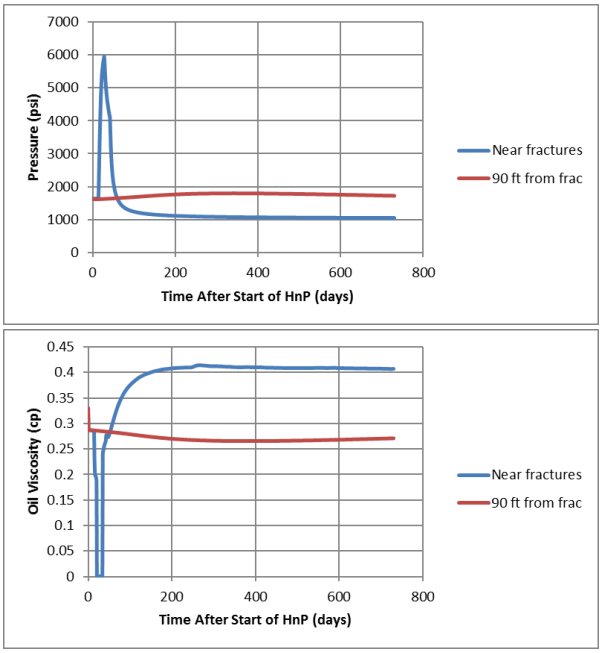

Figure 5.15: Pressure and oil viscosity vs time for two different locations within the reservoir.

Since a live oil model was used in this case, it was therefore necessary to investigate gas recovery as well as oil recovery. Figure 5.16 shows a plot of the gas-oil ratio (GOR) during primary and huff n' puff production. As the plot shows, GOR goes up as gas injection occurs, but then stabilizes between 25,000-30,000 scf/stb. During primary production, the GOR stabilized at around 170,000 scf/stb, meaning that huff n' puff reduced the GOR by over 80% while also recovering 10% incremental gas. An analysis on the composition of produced oil and gas was also executed. On average, the oil consisted mostly of the C7-9 and C10-13 pseudocomponents (over 75 mol%) in both primary and huff n' puff production while the gas consisted mainly of the lighter pseudocomponents. Oil composition did not change significantly after huff n' puff treatment, but there was a slightly lower molar amount of light components in the huff n' puff production.

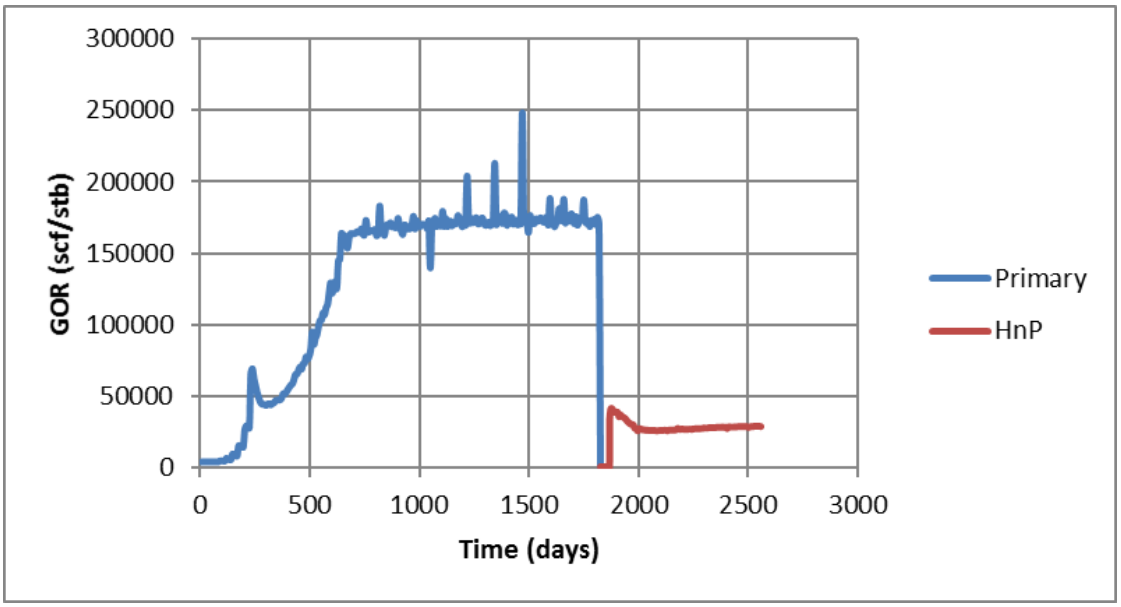

Figure 5.16: Gas-oil ratio (GOR) for primary and huff n' puff production

Although it was clearly shown that incremental oil could be recovered from a fractured nanodarcy LRS reservoir through recycled gas huff n' puff treatment, a sensitivity analysis was conducted using other injection fluids to test whether or not the proposed treatment is economical. The two additional cases had the same inputs as the proposed recycled gas treatment, but used water and propane as injection fluids. Propane is expected to mix better with the reservoir oil as illustrated in Table 5.6, while water is assumed to not mix with the oil at all. Figure 5.17 shows the incremental oil recovery for all three cases. As expected, propane significantly outperformed the recycled gas case. This was due to better mixing between the oil and gas and a decreased mobility ratio. However, the water case also outperformed the recycled gas case after two years of huff n' puff. This points to the fact that mixing might not be a significant performance parameter at all, but rather simply re-energizing the reservoir. When pressuring up the reservoir with water, water minimally imbibes into the matrix due to low injectivity. However, when switched to

production, oil is able to flow much easier than the water because of its low viscosity and favorable relative permeability. It is also important to note that the model was made to be completely water-wet, which may be an oversimplification considering the complexity of the shale matrix.

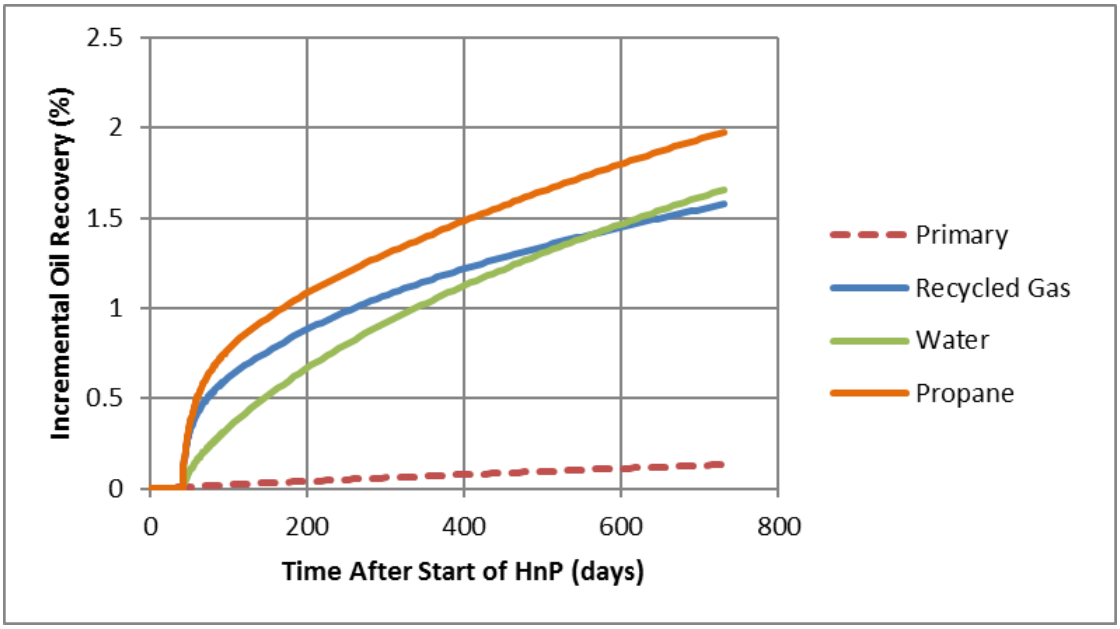

Figure 5.17: Incremental oil recovery for one huff n' puff treatment using three different injection fluids.

CHAPTER 6: CONCLUSIONS AND RECOMMENDATIONS FOR FUTURE WORK

In this body of work, oil recovery experiments and reservoir models were used to explore the use of recycled gas huff n' puff on a liquid-rich shale reservoir in order to enhance recovery. In the experimental portion, complex equipment, setup, and procedures were fabricated in order to determine whether or not oil could be recovered from reservoir shale samples with permeabilities less than 1 microdarcy, which very few have investigated up to this point in time. Propane was used in addition to the recycled hydrocarbon gas at different pressures in order to compare results. A compositional reservoir simulator was then used to create both lab- and field-scale models in order to further investigate the effects of pressure (injection and production) and injection gas.

6.1 Experimental Approach

The following are conclusions and recommendations for future work regarding the experimental portion of this work, which is described in Chapters 3-4:

1. Accurately quantifying oil recovery in shale samples with less than 1 mL of total oil is a very difficult task and requires unique methodology when compared to conventional coreflooding experiments. It was found that analyzing the shale samples and effluent with gas chromatography is an effective method. In future works, CT scanning technology (as used in Tovar et al, 2014) should also be used to be able to investigate fluid flow in the samples during experimentation.
2. The ability to directly measure permeability or any other sort of injection parameter (i.e. amount of gas being injected into the sample) requires highly complex experimental equipment that was not available for this work.

3. Five experiments in total were run. Shale samples were treated with two cycles of huff n' puff using the proposed recycled hydrocarbon gas and propane. Injection pressures were above MMP. Despite lower injection pressures, the propane experiments outperformed the recycled gas experiments. This is because propane mixes better with the oil and because production was run at a much lower pressure, pointing out the fact that injection pressure does not significantly affect performance as long as it is above MMP. However, production pressure does significantly affect results, especially if it is below the bubble point of the oil.
4. Extra huff n' puff cycles were run on several experiments with extended soaking times, but no additional oil was recovered in any of the cases. Because of this, it is concluded that convection was still the dominating mixing process in these experiments rather than diffusion. This could be due to the presence of natural fractures or anisotropy in the samples. In future works, samples cored at different angles with respect to the bedding plane should be used as well as samples with and without natural fractures.
5. Based on these results, it can be concluded that huff n' puff with the recycled hydrocarbon gas is a viable option for enhancing recovery when taking into account the low operating costs. Because the initial conditions were quite different in the experiments compared to depleted reservoir conditions, 15% incremental recovery is not to be expected in the field. However, it is estimated that even incremental recoveries as low as 1% could be cost-effective.

6.2 Compositional Modeling Approach

The following are conclusions and recommendations for future work regarding the experimental portion of this work, which is described in Chapter 5:

1. The results from the lab-scale models agree well with the oil recovery results seen in the experiments described in Chapter 4. In the base case, there was roughly half as much oil recovered as was recovered in the recycled gas experiments, which was expected considering the computational domain encompassed roughly half of the surface area seen in the experiments.
2. A lab-scale model was run with an elevated injection pressure of 5000 psi, but recovery did not increase. This proves what was seen in the experiments: as long as MMP is obtained, injection pressure does not significantly affect recovery.
3. Another lab-scale model was also run with a decreased production pressure of 1000 psi, resulting in a substantial increase in recovery. This also agrees with the experimental findings: lower production pressures allow for more gas expansion and therefore better recovery. This also proves that production pressure alone may be an important parameter rather than the ratio between production and injection pressures.
4. The field-scale models that were created in this work contained two hydraulic fractures with several natural fractures intersecting perpendicularly. A base case primary production model was first run and 12.76% of the original oil in place was recovered. It was decided that huff n' puff operations would begin after five years of primary production in order to preserve some of the initial reservoir pressure. The recycled gas model recovered approximately 1.5% incremental oil after a single huff n' puff cycle lasting just two years. The slope of the recovery curve was also increased, showing promise for further recovery after the two years.

5. The use of live oil in the field-scale models yielded vastly different results from the lab-scale models. It was shown that on top of increasing oil recovery, the huff n' puff treatment significantly decreased the GOR during production while also producing slightly heavier oil compared to primary production. It also showed that gas expansion caused by production below the bubble point of the oil significantly enhances performance of the huff n' puff treatment.
6. The model ran with propane as the injection gas significantly outperformed the recycled gas case due to enhanced mixing. The water case performed slightly better during the two years of production, showing that in the field-scale, re-energizing the reservoir might play a bigger role in recovery than mixing. However, the slopes of the recovery curves indicated that the recycled gas would likely outperform the water case given more time.
7. It is concluded that the main difference between lab- and field-scale huff n' puff operations is sweep efficiency. In the lab, the gas is able to contact most of the oil very quickly. This makes the fine-tuning of injection parameters (i.e. soaking time, soaking pressure, etc.) fairly insignificant compared to mixing parameters such as diffusion coefficients. However, in the field, mixing does not occur in the majority of the reservoir, but rather within several feet of fracture faces. This makes the injectivity of the gas and relative permeability model much more important. Higher injection pressures would likely increase recovery due to larger channels being created and therefore *more* mixing occurring.
8. Current compositional modeling software has various limitations that make modeling huff n' puff treatments in LRS reservoirs very difficult. For example, the assumption that complete mixing occurs within each gridblock differs significantly from what occurs in a LRS reservoir. However, the difficulty in developing new simulators that

model this process more accurately is that there is little experimental/field data to history match. Therefore, more experimental work that yields more data must be done to truly make the application of recycled gas huff n' puff a viable option in the field.

REFERENCES

Akhurt, R. et al.: "Nuclear Magnetic Resonance Comes Out of its Shell"; *Oilfield Review Winter 2008/2009: 20,* no. 4. 4-23

ASTM D2887-97a, "Standard Test Method for Boiling Range Distribution of Petroleum Fractions by Gas Chromatography", Annual Book of Standards, Volume 05.02, ASTM, 100 Barr Harbor Drive, West Conshohocken, PA 19428 USA.

Chen, C., Balhoff, M. T., & Mohanty, K. K. (2014, August 1). Effect of Reservoir Heterogeneity on Primary Recovery and CO2 Huff "n" Puff Recovery in Shale-Oil Reservoirs. Society of Petroleum Engineers. doi:10.2118/164553-PA

Chen, C., and D. Zhang (2010), Pore-scale simulation of density-driven convection in fractured porous media during geological CO2 sequestration, Water Resources. Res., 46, W11527, doi:10.1029/2010WR009453.

Clark, N. J., Shearin, H. M., Schultz, W. P., Garms, K., & Moore, J. L. (1958, June 1). Miscible Drive - Its Theory and Application. Society of Petroleum Engineers. doi:10.2118/1036-GCoats, K. H. (1989, January 1). Implicit Compositional Simulation of Single-Porosity and Dual-Porosity Reservoirs. Society of Petroleum Engineers. doi:10.2118/18427-MS

Clarkson, C. R., & Pedersen, P. K. (2011, January 1). Production Analysis of Western Canadian Unconventional Light Oil Plays. Society of Petroleum Engineers. doi:10.2118/149005-MS

Computer Modeling Group Ltd. (CMG). (2015) *User's Guide - GEM: Advanced Compositional and Unconventional Reservoir Simulator*. Calgary, Canada.

Computer Modeling Group Ltd. (CMG). (2015) *User's Guide - WinProp: Phase Behavior and Fluid Property Program.* Calgary, Canada.

Dao, E. K., Lewis, E. J., & Mohanty, K. K. (2005, January 1). Sweep Efficiency During Laboratory-Scale Multicontact Gas Flooding. Society of Petroleum Engineers. doi:10.2118/97198-MS

Fakcharoenphol, P., Charoenwongsa, S., Kazemi, H., & Wu, Y.-S. (2012, January 1). The Effect of Water Induced Stress to Enhance Hydrocarbon Recovery in Shale Reservoirs. Society of Petroleum Engineers. doi:10.2118/158053-MS

Fragoso, A., Wang, Y., Jing, G., & Aguilera, R. (2015, November 18). Improving Recovery of Liquids from Shales through Gas Recycling and Dry Gas Injection. Society of Petroleum Engineers. doi:10.2118/177278-MS

Gong, X., Tian, Y., McVay, D. A., Ayers, W. B., & Lee, J. (2013, November 5). Assessment of Eagle Ford Shale Oil and Gas Resources. Society of Petroleum Engineers. doi:10.2118/167241-MS

Hawthorne, S. B., Gorecki, C. D., Sorensen, J. A., Steadman, E. N., Harju, J. A., & Melzer, S. (2013, November 5). Hydrocarbon Mobilization Mechanisms from Upper, Middle, and Lower Bakken Reservoir Rocks Exposed to CO. Society of Petroleum Engineers. doi:10.2118/167200-MS

Hoteit, H. (2011, January 1). Proper Modeling of Diffusion in Fractured Reservoirs. Society of Petroleum Engineers. doi:10.2118/141937-MS

Hoffman, B. T. (2012, January 1). Comparison of Various Gases for Enhanced Recovery from Shale Oil Reservoirs. Society of Petroleum Engineers. doi:10.2118/154329-MS

Honarpour, M. M., Nagarajan, N. R., Orangi, A., Arasteh, F., & Yao, Z. (2012, January 1). Characterization of Critical Fluid PVT, Rock, and Rock-Fluid Properties - Impact on Reservoir Performance of Liquid Rich Shales. Society of Petroleum Engineers. doi:10.2118/158042-MS

Hoteit, H., & Firoozabadi, A. (2009, June 1). Numerical Modeling of Diffusion in Fractured Media for Gas-Injection and -Recycling Schemes. Society of Petroleum Engineers. doi:10.2118/103292-PA

Jamili, A. (2010). *Modeling Effects of Diffusion and Gravity Drainage on Oil Recovery in Naturally Fractured Reservoirs Under Gas Injection.* (PhD thesis) University of Kansas, Lawrence, Kansas, USA.

Kovscek, A. R., Tang, G.-Q., & Vega, B. (2008, January 1). Experimental Investigation of Oil Recovery From Siliceous Shale by CO2 Injection. Society of Petroleum Engineers. doi:10.2118/115679-MS

Lake, L.W., Johns, J. T., Rossen, W. R., and Pope, G. A. (2014) *Fundamentals of Enhanced Oil Recovery*. Society of Petroleum Engineers. ISBN 978-1-61399-328-6

Orr, Jr., F. M. (2007) *Theory of Gas Injection Processes*, First Edition. Tie-Line Publications. ISBN 87-989961-2-5

Railroad Commission of Texas – Eagle Ford Information. (2013). Retrieved December 4, 2015, from https://www.rrc.state.tx.us/eagleford/

Sanchez-Rivera, D. (2014) *Reservoir Simulation and Optimization of CO_2 Huff-and-Puff Operations in the Bakken Shale.* (Master's thesis) Austin, TX: The University of Texas at Austin

Sanchez-Rivera, D., Mohanty, K., Balhoff, M., 2015. Reservoir Simulation and Optimization of Huff-and-Puff Operations in the Bakken Shale, *Fuel*, 147, 82-94

Sun, J., Zou, A., & Schechter, D. (2016, April 11). Experimental and Numerical Studies of CO_2 EOR in Unconventional Liquid Reservoirs with Complex Fracture Networks. Society of Petroleum Engineers. doi:10.2118/179634-MS

Teklu, T. W., Alharthy, N., Kazemi, H., Yin, X., Graves, R. M., & AlSumaiti, A. M. (2014, August 1). Phase Behavior and Minimum Miscibility Pressure in Nanopores. Society of Petroleum Engineers. doi:10.2118/168865-PA

Tovar, F. D., Eide, O., Graue, A., & Schechter, D. S. (2014, April 1). Experimental Investigation of Enhanced Recovery in Unconventional Liquid Reservoirs using CO2: A Look Ahead to the Future of Unconventional EOR. Society of Petroleum Engineers. doi:10.2118/169022-MS

Vega, B., O'Brien, W. J., & Kovscek, A. R. (2010, January 1). Experimental Investigation of Oil Recovery From Siliceous Shale by Miscible CO2 Injection. Society of Petroleum Engineers. doi:10.2118/135627-MS

Wan, T., and Sheng, J. (2015, March 1). Compositional Modelling of the Diffusion Effect on EOR Process in Fractured Shale-Oil Reservoirs by Gasflooding. Society of Petroleum Engineers. doi:10.2118/2014-1891403-PA

Yu, Y., & Sheng, J. J. (2016, April 11). Experimental Evaluation of Shale Oil Recovery from Eagle Ford Core Samples by Nitrogen Gas Flooding. Society of Petroleum Engineers. doi:10.2118/179547-MS

Zhu, P., Balhoff, M. T., & Mohanty, K. K. (2015, September 28). Simulation of Fracture-to-Fracture Gas Injection in an Oil-Rich Shale. Society of Petroleum Engineers. doi:10.2118/175131-MS

VITA

Taylor Isbell was born in Louisville, Kentucky. In 2010, he entered the University of Kentucky, where he graduated with honors, receiving a B.S. in Chemical Engineering. In 2014, he entered the University of Texas at Austin pursuing a M.S. in Petroleum Engineering. Upon graduating in August of 2016, Taylor began work with Chevron Energy Technology Company as a Reservoir Engineer.

Permanent email: jtisbell4@gmail.com

This thesis was typed by Jordan Taylor Isbell